THESIS FOR THE DEGREE OF DOCTOR OF PHILOSOPHY IN NATURAL SCIENCE,
SPECIALIZATION IN CHEMISTRY

Molecular Investigations of Atmospherically Relevant Interface Processes

Ice Formation and Water Accommodation on Ice and Organic Surfaces

Xiangrui Kong

UNIVERSITY OF GOTHENBURG

Department of Chemistry
University of Gothenburg
Göteborg, Sweden, 2014

Molecular Investigations of Atmospherically Relevant Interface Processes: Ice Formation and Water Accommodation on Ice and Organic Surfaces

Department of Chemistry and Molecular Biology
Atmospheric Science
University of Gothenburg
SE-412 96 Sweden 2014-06

Printed by Aidla Trading AB
Göteborg, Sweden 2014

ISBN: 978-91-628-9024-7

Cover picture: Drawing of typical ice particles in cirrus clouds

Abstract

Clouds and aerosols play important roles in the climate system by affecting on atmospheric chemistry, the radiation budget of the atmosphere, and the water cycle including the formation of precipitation. Climate models with predictive power require quantitative descriptions of aerosols and clouds, but several key processes remain to be fully understood. One important example is the formation and growth of ice particles in clouds. Organic compounds also form secondary organic aerosol and coatings on existing particles including ice nuclei and ice cloud particles, which further complicate the description of cloud processes. To improve the understanding of these processes, some fundamental investigations of atmospherically relevant interface interactions are carried out, and the results and findings are summarized and discussed in this thesis.

The investigations use a newly developed environmental molecular beam (EMB) technique as the main experimental method. The principle, design and demonstration of the EMB method are described in detail. The method allows for ice surface investigations at temperatures up to 213 K, and it is employed to study gas-surface interactions under conditions relevant to the troposphere.

The main findings of this thesis are related to three research themes: (1) Ice formation via deposition mode nucleation on hydrophobic and hydrophilic surfaces is characterized. The critical supersaturation required to activate nucleation on various surfaces increases rapidly with decreasing temperature below 200 K, and adsorbed organic compounds are observed to influence the nucleation, structure and growth rate of ice. (2) Water uptake by bare ice and coated ice surfaces is investigated. The accommodation and desorption kinetics for water on bare ice is quantitatively described by a precursor model. Coatings on ice have a significant impact on water uptake, and adsorption of acids commonly found in the atmosphere tends to enhance water accommodation. (3) Water interactions with surfaces on condensed organic phases and organic coatings on graphite are characterized. Bulk accommodation is inefficient on solid organic surfaces, while water uptake is efficient on liquid phases. The surface layer on condensed *n*-butanol is shown to change gradually from solid to liquid over a 10 K temperature span around the bulk melting temperature, with major implications for water uptake.

The thesis includes the development of new experimental methods and an improved molecular-level understanding of processes at gas-solid and gas-liquid interfaces, and thereby contributes to a better description of cloud and aerosol processes in the environment.

Keywords: Environmental molecular beam (EMB), atmosphere, water, ice, organics, ice nucleation, deposition freezing, graphite, supersaturation, accommodation coefficient, deposition kinetics, collision dynamics, phase transition, alcohols, acetic acid, nitric acid, environment, green chemistry

List of publications

Paper I

Environmental molecular beam studies of ice surface processes

Xiangrui Kong, Patrik U. Andersson, Nikola Markovic, and Jan B.C. Pettersson

Proceedings of the 12th International Conference on the Physics and Chemistry of Ice, Hokkaido University Press, Sapporo, 2011, 79-88.

Paper II

Ice Formation via Deposition Mode Nucleation on Bare and Alcohol Covered Graphite Surfaces

Xiangrui Kong, Patrik U. Andersson, Erik S. Thomson, and Jan B. C. Pettersson

Journal of Physical Chemistry C, 2012, 116 (16), 8964–8974.

Paper III

Deposition mode ice nucleation reexamined at temperatures below 200 K

Erik S. Thomson, Xiangrui Kong, Panos Papagiannakopoulos, Nikola Markovic, and Jan B.C. Pettersson

Manuscript for Atmospheric Chemistry and Physics.

Paper IV

Water Accommodation and Desorption Kinetics on Ice

Xiangrui Kong, Panos Papagiannakopoulos, Erik S. Thomson, Nikola Markovic, and Jan B.C. Pettersson

Submitted to Journal of Physical Chemistry A.

Paper V

Collision Dynamics and Solvation of Water Molecules in a Liquid Methanol Film

Erik S. Thomson, Xiangrui Kong, Patrik U. Andersson, Nikola Markovic, and Jan B. C. Pettersson

Journal of Physical Chemistry Letters, 2011, 2 (17), 2174–2178.

Paper VI

Water Interactions with Acetic Acid Layers on Ice and Graphite

Panos Papagiannakopoulos, Xiangrui Kong, Erik S. Thomson, and Jan B.C. Pettersson

Submitted to Journal of Physical Chemistry B

Paper VII

Surface Transformations and Water Uptake on Liquid and Solid Butanol near the Melting Temperature

Panos Papagiannakopoulos, Xiangrui Kong, Erik S. Thomson, Nikola Markovic, and Jan B.C. Pettersson,
Journal of Physical Chemistry C, 117 (2013) 6678-6685.

Paper VIII
Collision Dynamics and Uptake of Water on Alcohol-covered Ice
Erik S. Thomson, Xiangrui Kong, Nikola Markovic, Panos Papagiannakopoulos, and Jan B.C. Pettersson
Atmospheric Chemistry and Physics, 13 (2013) 2223-2233.

Paper IX
Water Accommodation on Ice and Organic Surfaces: Insights from Environmental Molecular Beam Experiments
Xiangrui Kong, Erik S. Thomson, Panos Papagiannakopoulos, Sofia Johansson, and Jan B.C. Pettersson
Submitted to Journal of Physical Chemistry B

Table of Contents

List of Abbreviations

α	*Accommodation Coefficient*
α_b	*Bulk Accommodation Coefficient*
α_s	*Surface Accommodation Coefficient*
α_t	*Thermal Accommodation Coefficient*
CNT	*Classical Nucleation Theory*
DSMC	*Direct Simulation Monte Carlo*
EMB	*Environmental Molecular Beam*
ESEM	*Environmental Scanning Electron Microscopy*
GISANS	*Grazing incidence small-angle neutron scattering*
HOPG	*Highly Oriented Pyrolytic Graphite*
IS	*Inelastic Scattering*
MB	*Molecular beam*
MD	*Molecular Dynamics*
NASA	*National Aeronautics and Space Administration*
NEXAFS	*Near Edge X-Ray Absorption Fine Structure*
QLL	*Quasi Liquid Layers*
QM	*Quantum Mechanics*
QMS	*Quadrupole Mass Spectrometer*
RS	*Raman Spectroscopy*
SEM	*Scanning Electron Microscopy*
SHG	*Second-Harmonic Generation*
S_i	*Critical Supersaturation Ratio*
SOA	*Secondary Organic Aerosol*
SPR	*Surface Plasmon Resonance*
STM	*Scanning Tunneling Microscopy*
TD	*Thermal Desorption*
TOF	*Time-Of-Flight*
UHV	*Ultra-High Vacuum*
XRD	*X-Ray Diffraction*
XPS	*X-Ray Photoemission Spectroscopy*

Chapter I

Introduction

Simplicity is the beauty of science.
Sometimes it comes with a theory, like Einstein's equation $E = mc^2$;
Sometimes it lies in an experiment, like Young's double-slit setup;
And sometimes it is just about a matter, like ***water****.*

The behavior and role of water on Earth was described by the Greek philosopher Aristotle as early as the fourth century BC[1], but even now we can only partially answer many questions concerning water in its gas, liquid or solid forms. Solid water makes up snow, glaciers, sea ice and also clouds (often mixed with water droplets) on Earth. Clouds influence the radiation budget of the atmosphere through scattering and absorption of radiation and affect the water cycle through the formation of precipitation. However, the formation and properties of clouds are main uncertainties that influence the quality of climate predictions in the context of modern research on climate change. One particular uncertainty influencing cloud predictions is the effects of emitted organic compounds, which may alter the formation, life cycle and properties of clouds.

In this thesis, I seek to improve the fundamental understanding of atmospherically relevant interface processes, such as ice formation and water uptake by ice and organic surfaces. The investigations are bawd on the application of a newly developed molecular level experimental technique, termed the environmental molecular beam (EMB) method. The EMB method partially overcomes the pressure limitations of traditional molecular beam techniques, allowing us to study ice under upper conditions relevant to the troposphere.

Nine published papers or submitted manuscripts connected as shown in Figure 1.1 are included in this thesis. Paper I stands on the top of the figure because it presented the development of the EMB technique that has been used as the primary experimental tool for the entire course of study, and as the basis for the other papers. The papers in the left column focus on water ice, which includes ice formation via deposition freezing (Paper II), measured critical supersaturations for deposition nucleation (Paper III) and water accommodation on pure ice (Paper IV). These three papers discuss in some detail ice formation and growth in terms of important parameters relevant to the atmosphere. The manuscripts in the right column focus on systems involving various organic compounds with graphite and/or ice. Organic coatings on graphite and bulk organics have been studied in terms of their interactions with water. The effect of coatings of these compounds on water uptake

by ice are discussed and compared to the pure ice case. Paper IX summarizes the findings of water accommodation on ice and organics surfaces from earlier papers with complementary new data. The dashed lines indicate the interlinked papers. The use of the three colors is to emphasize the three main parts of this thesis, which are ice formation (red), water uptake by ice (blue) and water interactions with organic surfaces (green).

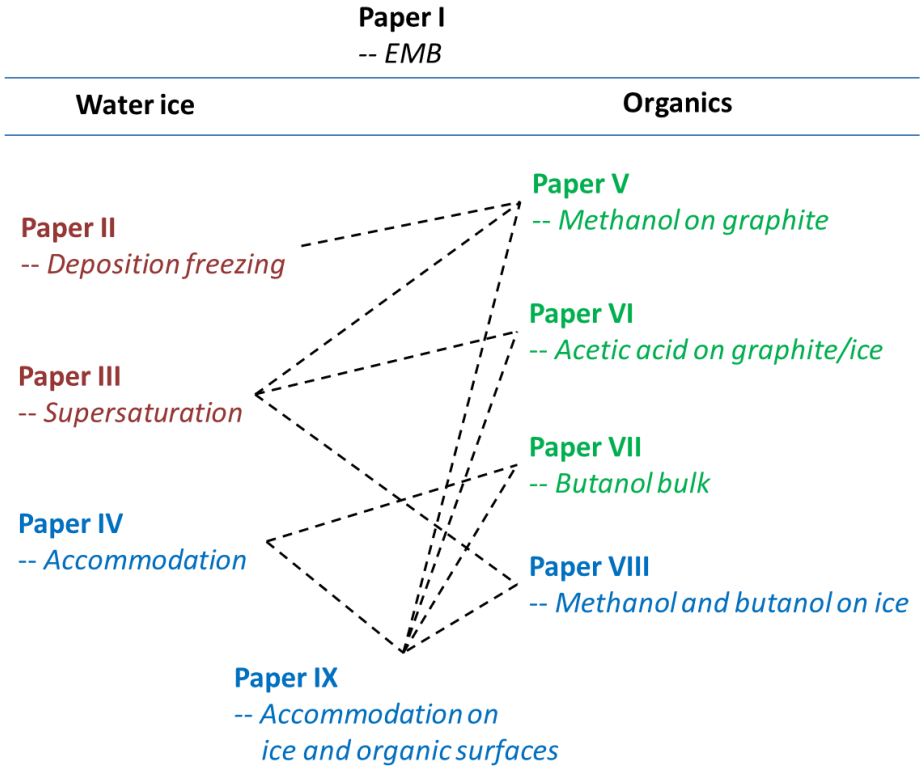

Figure 1.1 Clustering and linkage of included papers

Several important issues related to ice particles and organics surfaces in the atmosphere will be stressed in this thesis. The molecular level investigations improve the fundamental scientific understanding of the surface properties of water ice and organic aerosols, which may serve as a basis for a good comprehension of our climate system.

Chapter II

Background

2.1 Water ice

Water is a unique natural substance in that it co-exists in its three phases in the typical temperature range at the Earth's surface (see Figure 2.1). Liquid water has many peculiar physical properties differing from most other liquids, e.g. a high surface tension, a high specific heat capacity, a maximum density at 4 ºC at standard atmospheric pressure, a lower viscosity under high pressure[2], etc. As the solid form, ice has its own extraordinary properties. Taking a famous but probably not very scientific example from the early history, Aristotle wrote in his treatise *Meteorology* that warm water could freeze faster than cold water, though his explanation is more philosophic than scientific[1]. However, for the public such confusion still remains even in modern time, and similar findings have been reported[3,4]. Actually, if looking into such a phenomenon in a strict scientific way, the fact is not mysterious anymore because the water phase transition is indeed of complexity and sensitivity. Temperature is just one parameter out of many to influence water freezing, and the other factors include pressure, cooling rates, fluid turbulences, nuclei concentrations, trace chemical compositions, and so on.

Figure 2.1 Hot spring Blue Lagoon in Iceland. Although only liquid water is physically visible in this picture, it is expressive of all three water phases: the steam is made of **LIQUID** droplets formed by condensation of water **VAPOR**, and the picture was taken in **ICE**land.

Another popular and interesting question regarding ice is why the surface is slippery. It is known that it is due to a liquid layer existing on the top of the ice surface. For example, during skating there is a Lubricating layer between the blades and the ice

surface. However, one may wonder how the liquid layer can form when the temperature is below 0 ºC, e.g. optimum temperatures for figure skating is -5.5 ºC and for ice hockey -9 ºC[5]. Some hypotheses have been proposed to explain this, such as the pressure melting theory[6] and the friction heating theory[7], but they fail to explain skating at very low temperatures (e.g. it is possible to skate at -30 ^{0}C or even lower) and slipperiness without friction (e.g. the ice surface is still slippery when you stand still on it). Actually, as early as in the 19th century, Faraday proposed that a liquid-like layer exists on ice surface already below the melting temperature. He was inspired by the fact that two thawing pieces of ice adhere and become one when they are put in contact with each other[8]. By modern scientific techniques, such layers have been confirmed[9] and termed as disordered or quasi-liquid layers (QLLs).

2.2 Water ice in the atmosphere

Ice formation in the atmosphere requires low temperatures. When talking about low temperatures, we may immediately think of the Artic or Antarctic; and when talking about ice in the atmosphere, snowflakes come into mind. However, if we abandon ground level thinking, the picture changes thoroughly. For example, at an altitude of 10 km atmosphere temperatures are always cold, near -50 ^{0}C, which is low enough to form ice clouds if the vapor pressure and other factors are suitable.

Cirrus clouds (Figure 2.2) are ice clouds that are of special interest in this thesis. Lying in the upper parts of the troposphere, cirrus clouds cover 20-30% of the global sky[10-12], and therefore impact the radiation budget of Earth[13,14]. The optical properties of cirrus vary depending on the size[15], shape[16,17], and surface roughness[18] of the

Figure 2.2 Cirrus clouds (Picture from Wikipedia)

cloud's ice particles. Thus, a good understanding of the formation and properties of these ice particles is beneficial when describing the climate system. Ice particles can be formed from homogeneous and heterogeneous freezing modes in the atmosphere. When pure water crystalizes without help from impurities or surfaces, it is called

homogeneous nucleation[19]. Homogeneous nucleation requires lower temperatures or high vapor saturations compared to heterogeneous nucleation[20-23], which is facilitated by ice nuclei[24]. There are four different sub-modes for heterogeneous nucleation, which are deposition mode, condensation mode, immersion mode and contact mode freezing[24-26]. Deposition freezing is important for ice particle formation in the upper troposphere where water vapor can directly deposit onto aerosol particles[27], and in this thesis all ice specimens were formed by deposition of vapor on substrates.

The critical vapor supersaturation required for heterogeneous nucleation is directly relevant to the quantification of cloud formation, but current estimates are far from agreeing on parameter values[28]. Depending on the properties of the heterogeneous surfaces, the required supersaturation ratio varies. Generally hydrophobic surfaces suppress nucleation compared to hydrophilic surfaces. In the atmosphere, particle surfaces are also commonly coated by impurities, and the hydrophilicity is consequently often altered. Below 200 K, the critical supersaturation critical supersaturation increases rapidly with decreasing temperature, though not many studies of this interesting phenomenon have been carried out[20,21,29,30].

After nucleation has occurred, the growth and change of ice particles are also difficult to describe and predict[23]. One reason is that the uptake process of gas water molecules by ice surfaces is not well constrained. In addition, there are many impurities in the atmosphere that may influence the uptake processes especially given that most heterogeneous compounds prefer to concentrate on the ice surface instead of being embedded into the ice bulk.

2.3 Organic aerosols in the atmosphere

Organic compounds in the atmosphere influence climate and air quality in various ways. All the processes previously mentioned regarding ice particle formation and growth can be influenced by the presence of airborne organics, and their effects are not well understood. On the other hand, atmospheric organics largely participate in aerosol formation to produce secondary organic aerosol (SOA) and coatings on existing particles[31]. Figure 2.3 illustrates the global aerosol distribution with classification of aerosol types. A large portion of sulfate particles (indicated in white color) is emitted by anthropogenic sources, and strong correlates to organic compounds. Their health impact is a primary issue in current air quality research. Studies of organic surfaces and their interactions with water are motivated by their roles in climate change and air pollution.

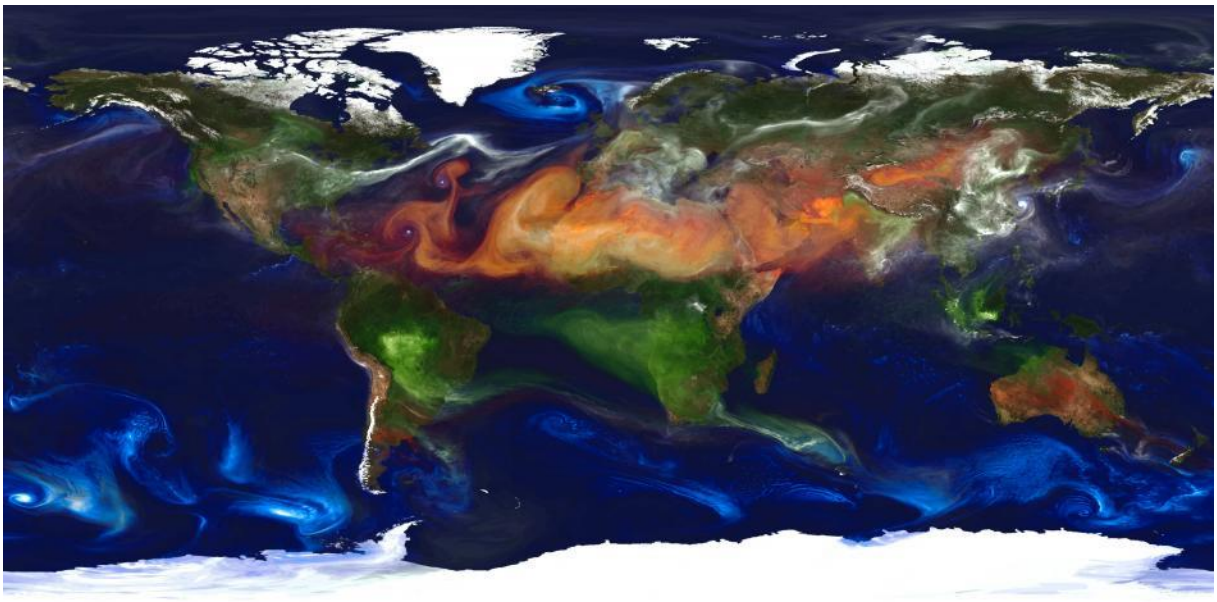

Figure 2.3 Mineral dust in red, sea salt in blue, smoke from fire in green, sulfate particles from natural sources and fossil fuel emissions in white. Portrait of global aerosols by NASA[32].

Chapter III

Experimental methods

Obtaining a molecular-level understanding of surface structures and processes requires powerful experimental techniques. Subatomic particles, such as photons and electrons, are often used as probes due to the excellent sensitivities that can be achieved and their penetrating ability. Atoms and molecules have larger sizes than subatomic particles, and thus they often require vacuum conditions to avoid attenuation by background gas. However, the atoms and molecules based methods have unique advantages in molecular dynamics and kinetics studies. In the following section, several commonly used surface-sensitive experimental techniques will be briefly introduced as a way of contextualizing and motivating the EMB method that was developed and used in our laboratory.

3.1 Common surface sensitive experimental techniques

Surface second-harmonic generation (surface SHG) is an experimental tool utilizing an electromagnetic phenomenon, whereby two photons with identical frequencies transform to one new double-frequency photon during interactions with a surface[33]. The output radiation is governed by a surface polarization in a way that depends on the surface susceptibility tensor[34], which indicates properties of the surface like the orientation of interfacial molecules. Thus, surface SHG has high surface sensitivity, and can be run without ultra-high vacuum conditions because of the excellent gas penetration ability of photons[35]. However, this method usually probes static surface conditions, unless repeated over time, in which case kinetic information can also be obtained.

Surface plasmon resonance (SPR) and ellipsometry both probe surface conditions using the refractive indices at liquid/solid interfaces. The two methods differ in that SPR monitors the interface through the solid, while ellipsometry is used from the liquid side of the interface, where another gas/liquid interface is also normally involved. Because of the interest in QLLs on ice surfaces, ellipsometry has been used to measure QLL thicknesses[36-38].

Raman spectroscopy (RS) extracts vibrational information from molecules using photon inelastic scattering from the electron cloud of molecular bonds. The wavenumber region related to OH bond stretching, indicating water structure, is covered by the RS wavenumber region[39], and the technique has been used to study water and ice since the 1960s[40].

High energy photons are also frequently used. X-ray diffraction (XRD) is based on the interference of incident X-rays caused by atomic crystal planes and is used to determine crystalline structure[41]. X-ray photoemission spectroscopy (XPS) is another highly surface sensitive method used to determine the elemental composition of surfaces[42,43], whereby incident high energy X-ray photons stimulate electrons to escape. Near edge X-ray absorption fine structure (NEXAFS) also irradiates surfaces with X-rays. In NEXAFS, the photons are adsorbed and fluorescence photons or electrons are emitted. This method is sensitive to the hydrogen bonds of water molecules, and it is applied to study water in different phases[44]. Recently, both XPS and NEXAFS have been used to study adsorbed compounds and ions on ice surfaces[45,46].

Electrons are another powerful probing medium sensitive to surfaces. Relevant techniques including scanning electron microscopy (SEM) and scanning tunneling microscopy (STM) have been used to visualize surface configurations of ice crystals[47] and layers[48]. Traditional SEM requires vacuum conditions, and for volatile substances like ice at environmental temperatures ($\geq$ 150 K), the target surface must be in a separated high-pressure chamber, while the electron source should be differentially pumped to maintain vacuum conditions. This method is termed environmental scanning electron microscopy (ESEM)[49].

Neutron diffraction has also been used for studying hydrogen positions in ice structures since 1949[50], and grazing incidence small-angle neutron scattering (GISANS) provides information about the surface roughness, lateral correlations, sizes and shapes of small objects, such as nanoparticles[51].

The techniques mentioned above have high surface sensitivity and provide information on surface shape, phases, elementary composition, molecular orientations, chemical bonds and hydrogen bonds. They are usually less well suited for characterization of fast dynamics and kinetics on the molecular level. Molecular beam (MB) methods originated in the early 20th century[52], and have been continuously developed since. In 1986, Dudley R. Herschbach and Yuan T. Lee were awarded the Noble prize in chemistry together with John C. Polanyi for their contributions concerning the dynamics of chemical elementary processes[53]. The MB method is one of the main experimental techniques used to experimentally study the fundamental processes of physical and chemical interactions. Currently, the definition of molecular beam is general, where the beam can be made of atoms, molecules or clusters, and the interactions between beam/solid surface[54], beam/liquid surface[55], beam/beam[56], and beam/gas[57] are all in the scope of MB. However, in the field of ice research the application of MB methods has been limited, especially at ice temperatures above 150 K[58-60]. That temperature is, however, too low for conditions of tropospheric relevance. Thus, further improvements of the method were carried out in the early stage of my studies, leading to the new refined technique termed

environmental molecular beam[61] that has been used as the primary experimental method for all of the work included in this thesis.

3.2 The EMB technique

The principle of the EMB technique is taken directly from traditional MB methods. A gas is let into a vacuum system and forms a directed low density flow of molecules called a MB. Because the molecular beam can be easily attenuated by scattering with background gas molecules, high-vacuum conditions are usually required in MB methods. Figure 3.1 shows the schematic view of the EMB apparatus. Gas pulses are generated from a gas source, with the central part of the pulse passing through a skimmer to form a directed beam with a diameter of 3 mm. Next, a rotating chopper modulates the gas pulses into square wave like beam pulses with a frequency selected width (typical used frequencies are 8 Hz and 120 Hz) before the beam enters

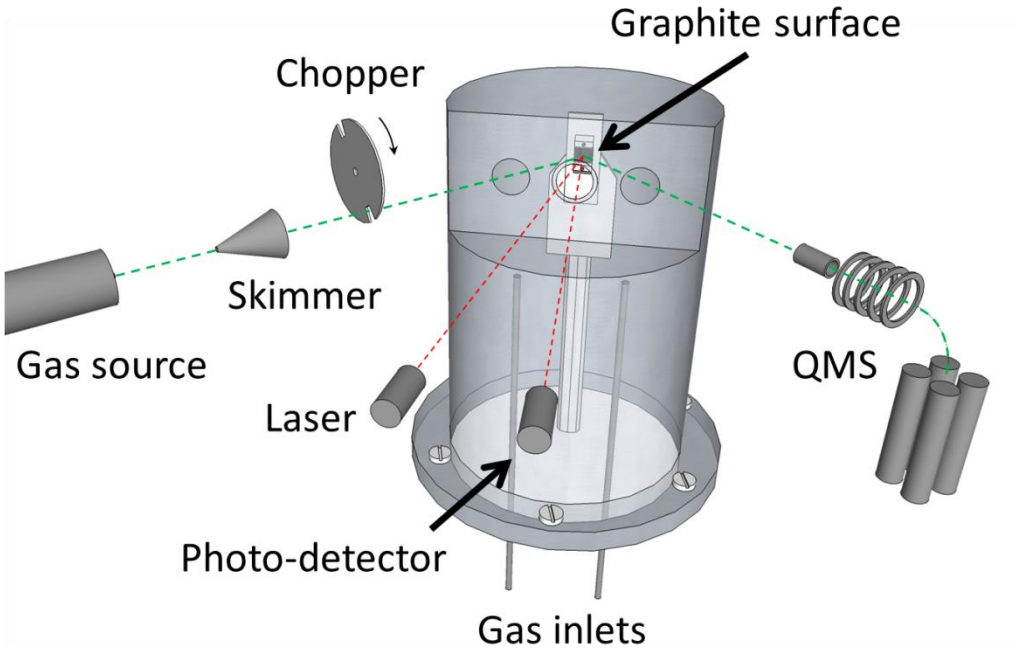

Figure 3.1 Schematic view of the EMB apparatus including the main components and the environmental chamber surrounding the surface The molecular beam is marked in green, and the laser beam in red.

a UHV chamber with a background pressure of 10^{-9} mbar. A sample surface is located in the center of the UHV chamber, surrounded by an environmental inner chamber. Two gas inlets end within this inner chamber; one is typically used for water vapor and the other is for other compounds of interested. Highly oriented pyrolytic graphite (HOPG, Advanced Ceramics Corp., grade ZYB) is used as a substrate surface, which can be covered by deposition from the vapor. The surface temperature is monitored by K-type thermocouples and controlled by a combined liquid-nitrogen cooling and electrical heating. A rotatable differentially pumped

quadrupole mass spectrometer (QMS) is used to measure both in the incident beam and in the flux from the surface.

3.3 Development of the EMB method

Traditional MB methods cannot be used to study ice surfaces at temperatures above 150 K because the ice evaporates rapidly in vacuum conditions. In order to maintain the ice, a finite vapor pressure has to be applied above the surface, providing enough condensable gaseous molecules to balance evaporation and adsorption. Because the equilibrium pressure of ice increases exponentially with temperature, beam attenuation can become very significant with even a small elevation of temperature. In the EMB method, this problem is solved to a large extent by the inclusion of the environmental chamber and the highest temperature for ice study herein reaches 213 K[62]. The additional environmental inner chamber surrounding the sample surfaces allows for an elevated pressure around the ice surface, while simultaneously the beam path length within the high pressure region is minimized in order to reduce beam attenuations.

The design of the inner chamber was evaluated by Direct Simulation Monte Carlo (DSMC) calculations, which is a numerical method for modeling rarefied gas flows in which the mean free path of gas molecules are of the same order or greater than the representative physical length scale[63]. The method models vapor flow using simulation molecules that represent a large number of real molecules in a probabilistic simulation that solves the Boltzmann equation[63]. Key computational assumptions associated with the DSMC method are the decoupling of the motion

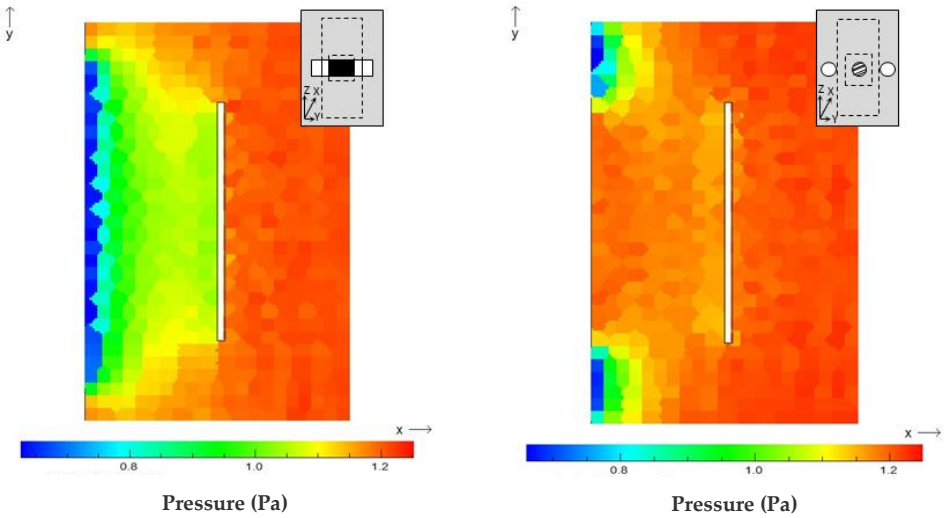

Figure 3.2 Steady-state pressure near the surface (white area) and the openings into the UHV chamber (blue regions) obtained by 3D DSMC calculations for two opening geometries. The insets show the view along the x-axis, where the grey rectangles represent the wall with holes or a slit, the large dashed rectangles are surface holders behind the plate, the small dashed rectangles are graphite surfaces behind the plate (the visible part is shown in black). In the right-hand case the shadowed circle is a quartz window. See Paper I for further details.

and collisions of the particles over small time steps and the division of the flow field into small cells. The time step should be much smaller than the mean collision time and a typical cell dimension should be much smaller than the local mean free path. The DSMC method is ideally suited for the present problem where the conditions near the opening between the two chambers change from a low pressure to vacuum. Two- and three- dimensional versions of the DSMC program[64,65] were employed for the design studies. The 2D version was used for rapid evaluation of different simplified geometries while the 3D version was needed for a detailed evaluation of the most successful 2D designs. Two examples of DSMC calculations resulting from this study are shown in Figure 3.2, which compares the pressure gradients in two inner chamber designs. The left panel illustrates the case where the inner chamber has a rectangular opening, and the right panel is for an inner chamber with two circular openings. The distance between the surface and the plate with the openings is 10 mm in the two cases. The color indicates the pressure distribution once a steady state has been reached in the simulations. From the comparison it is clear that higher pressures above the surface are better maintained when the chamber is engineered with small circular openings. In the left-hand case the pressure above the surface is less evenly distributed (shown in paper I). This is a critical drawback because ice will first grow in regions of high pressure, potentially altering the shape of the ice surface. The right-hand case in Figure 3.2 has a minor pressure difference of less than 1% over the entire surface area, and this design was used for the construction.

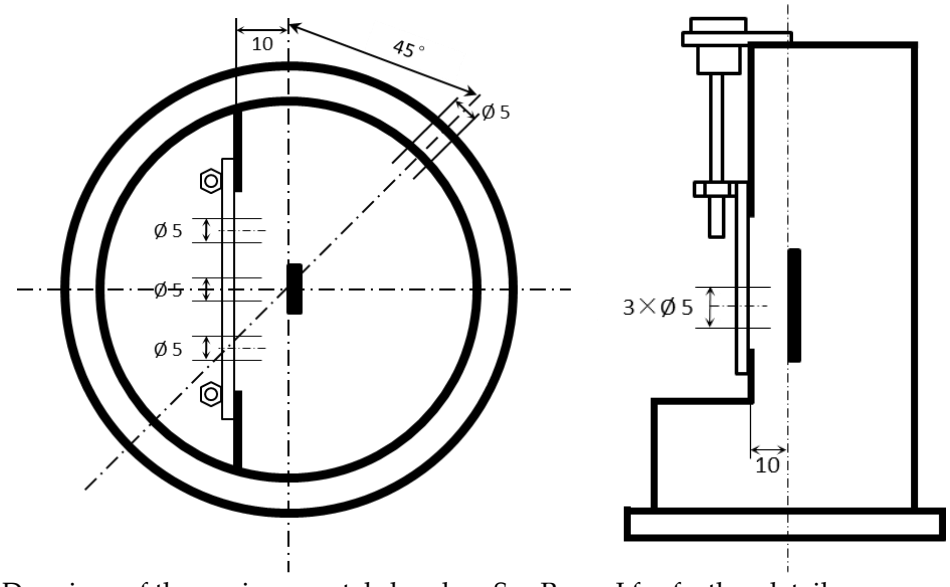

Figure 3.3 Drawings of the environmental chamber. See Paper I for further details.

The environmental chamber design is shown in Figure 3.3. The incident beam is allowed into the inner chamber through a thin circular opening with a diameter of 5 mm and collides with the surface at an angle of 45^0. The outgoing flux passes through a second opening and is measured in the specular direction. The distance between the surface and the inner chamber wall is 10 mm, and therefore the

measured molecules travel a total distance of 28 mm in the high pressure zone. A quartz window directly in front of the graphite surface allows light reflection measurements to be made using a continuously monitored laser beam focused on the surface at near normal incidence.

3.4 Demonstration of the new apparatus

After mounting the new inner chamber, several experiments were carried out to test the functionality of the new system. First the molecular beam transmission was tested under various water vapor pressures to determine the accessible range. Elastic surface scattering of helium atoms from clean graphite was used. Figure 3.4 shows the experimental helium transmission data plotted together with results from DSMC and quantum mechanical (QM) calculations. The transmission from all three curves drops quickly for vapor pressures higher than 10^{-3} mbar. In practice, a normalized transmission factor as low as 0.05 is acceptable for experiments, and thus the highest applicable pressure is approximately 1×10^{-2} mbar. Detailed discussions are included in Paper I.

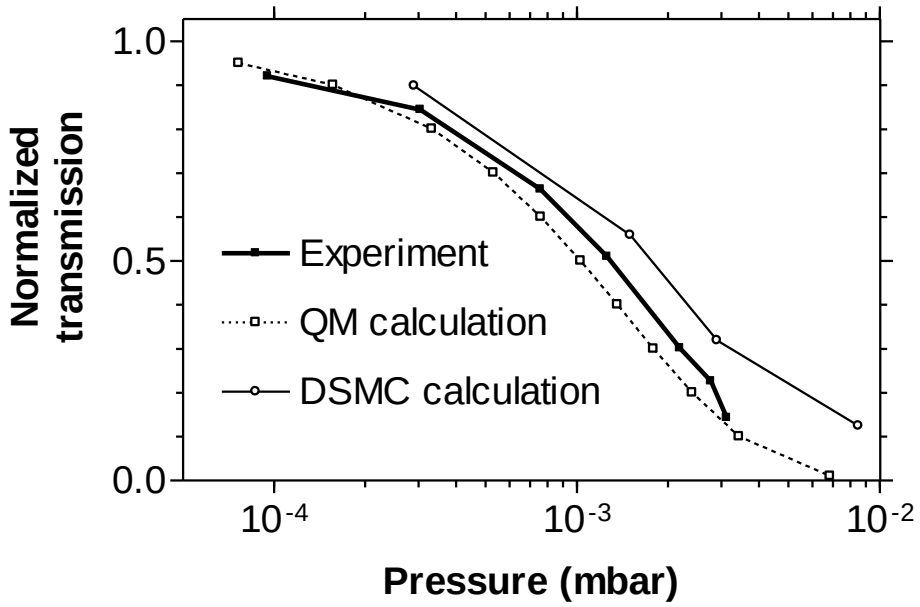

Figure 3.4 Helium transmissions as a function of pressure in the environmental chamber, see text and Paper I for further details.

3.5 Typical EMB data and analysis

The data typically obtained using the EMB method is time-resolved intensities of beam molecules scattered and desorbed from a surface. In studies of ice formation, helium atoms are used in the beam to probe surface coverage because they have a high probability for elastic scattering from bare graphite, while it is low from adsorbed layers[66,67]. Elastic scattering occurs when beam molecules do not exchange energy with surface molecules during collisions. For a flat surface, the beam scatters in the specular direction. A typical example of low kinetic energy helium elastically

scattering from a graphite surface is shown in Figure 3.5. Here the helium intensity declines as the graphite surface is gradually covered with water.

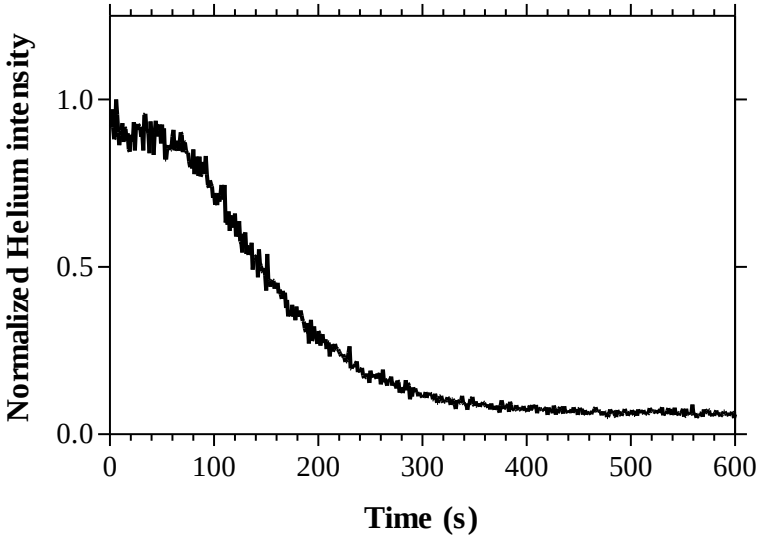

Figure 3.5 A typical helium intensity curve when graphite is gradually covered with water.

In studies of interactions between molecules and surfaces, time-of-flight (TOF) data are obtained using a multichannel scaler with a high time resolution. Figure 3.6 shows an example of typical TOF data of D_2O scattered and desorbed from a butanol multilayer at 184 K. The data are fitted with a non-linear least-squares two-component distribution, where the first distribution is inelastically scattered water and the second is thermally desorbed water from the surface. The inelastic scattering refers to partial energy exchange between molecules and the surface in collisions, while trapping-desorption refers to molecules that fully thermalize to surface temperatures before desorbing in random directions. The inelastic scattering (IS) and thermal desorption (TD) distributions have been characterized in order to fit the data points. The IS component is assumed as[68],

$$I_{IS}\big(v(t)\big) = C_1 v(t)^4 exp\left[-\left(\frac{v(t)-\bar{v}}{v_{IS}}\right)^2\right], \quad (1)$$

where C_1 is a scaling factor, $v(t)$ is the velocity calculated from time t and the path length between the surface and the QMS detector, $\bar{v}$ represents the peak of the inelastically scattered velocities, and v_{IS} is,

$$v_{IS} = (2k_b T_{IS}/m)^{1/2}, \quad (2)$$

where the temperature T_{IS} describes the velocity spread, k_b is the Boltzmann constant, and m is the molecular mass. The TD distribution takes the form of a residence time behavior,

$$F = C_2 \exp(-kt)\,, \tag{3}$$

where C_2 is a scaling factor, k is the desorption rate constant.

D_2O is used in the MB instead of H_2O to improve the signal-to-noise ratio. HDO is never detected in the emitted flux and isotopic exchange between D_2O and surface molecules can be ignored on the experimental time scale.

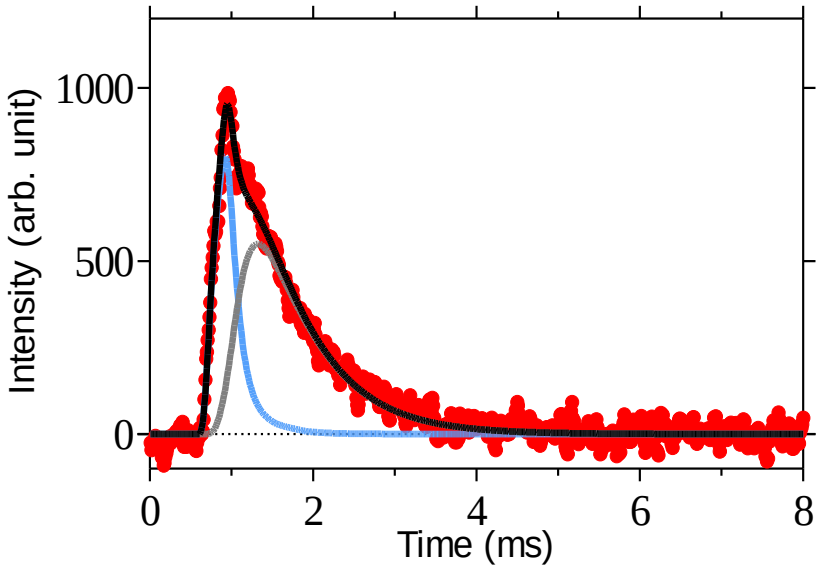

Figure 3.6 Typical TOF data for water scattering and desorbing from a butanol multilayer at 184 K. The red points are measured data. The black line is a non-linear least squares fit to the data, where the blue and grey lines are the inelastic scattering and thermal desorption components, respectively. See Paper VII for further details.

3.6 Layer thickness and roughness measurements

In addition to the MB method, the thickness of an ice layer can be monitored by laser interference measurements[69,70]. A laser is directed at the surface with an incident angle of 3°, and the reflected intensity in the specular direction is measured using a photon detector. As the ice layer grows a sinusoidal-like time variation in scattered intensity is produced by the constructive and destructive interference of light reflected by the ice layer and the underlying ice-graphite interface. Using the wavelength of the laser (λ), the incident angle (θ) and refractive index of ice (n), the ice thickness can be calculated using Equation (4), to determine the thickness at succeeding interference maxima,

$$d = m\,\lambda\,/\,2n\cos\theta,\ \mathrm{m} = 1, 2, 3\ldots \tag{4}$$

where the integer m represents the order of the maximum. In the temperature range 100 K - 200 K, the value of n is approximate 1.31[71]. Figure 3.7 shows typical light scattering data obtained during buildup of a smooth water ice surface. For each period, the corresponding increase in thickness of water ice is about $\lambda / 2n \approx 252$ nm, or 750 monolayers (ML) if each ice bilayer is considered to have a thickness of 3.4 Å[70,72].

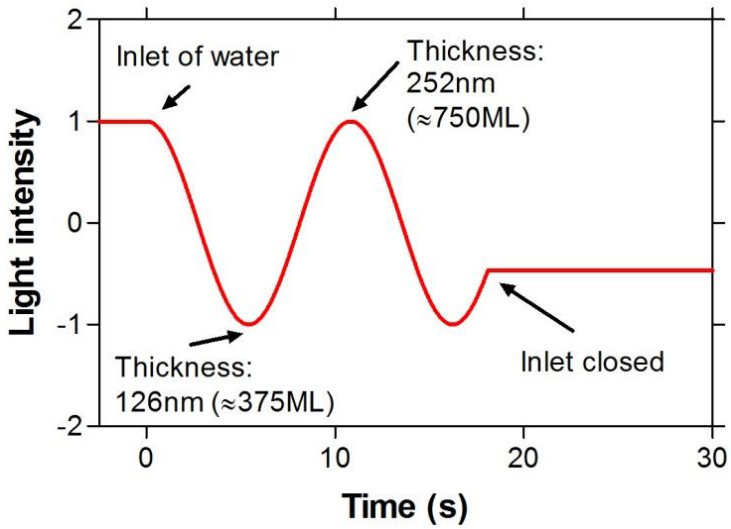

Figure 3.7 Typical light interference pattern during buildup of a flat water ice surface.

From non-smooth ice surfaces the surface roughness will attenuate reflected light intensity because of light scattering in other directions, and the evolution of surface morphology has been quantified using a surface roughness model that is described in detail in Paper II.

Chapter IV

Results and discussion

The main findings are presented in three subsections: 4.1 Ice formation via deposition freezing; 4.2 Water uptake by bare ice and coated ice; 4.3 Water interactions with organic surfaces.

4.1 Ice formation via deposition freezing

The investigation of ice formation under upper tropospheric conditions was a major motivating factor for building the EMB apparatus. Thus ice formation at temperatures up to 213 K will be illustrated to show the function of the EMB. The graphite surface is hydrophobic, but can be altered by organic coatings. Furthermore, to quantify ice formation it is necessary to determine the critical nucleation ratio S_i, and an attempt to link measured S_i with predicted values using classical nucleation theory will be described.

4.1.1 Water deposition freezing on a hydrophobic surface

Figure 4.1 illustrates two examples of ice formation and sublimation on graphite at 195 K and 213 K, where the helium intensity (I_{He}) and light intensity (I_R) are related to the ice coverage and the ice layer thickness, respectively. The high probability of

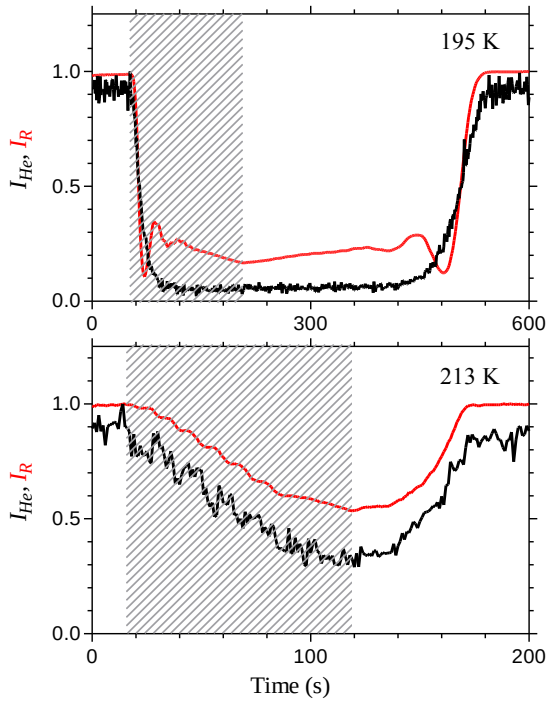

Figure 4.1 Water ice formation on graphite at 195 K and 213 K: normalized scattered helium intensity I_{He} and reflected light intensity I_R as a function of time. The shadowed areas indicate when the water inlet is on. See Paper II for further details.

helium elastic scattering from graphite allows for monitoring the surface coverages, and this is a primary reason for using graphite as the substrate. The shadowed areas show the period when the water vapor source was turned on, and consequently the graphite surface was covered with growing ice by water vapor deposition. It is worthwhile to notice that before the graphite surface is completely covered by ice (when the helium intensity reaches steady level) the light scattering attenuation indicates a substantial amount of surface roughness. This implies that water forms three dimensional ice-island structures on the graphite surface, in agreement with other studies[73,74]. The hydrophobicity of the graphite surface[75] means that the self-attraction of the water is greater than its attraction to the underlying graphite[70,76-78]. When the water value is turned off, the ice layer begins to shrink, and the helium and light intensities indicate that the ice adsorption and desorption processes are largely reversible.

4.1.2 Surfactant effects

The hydrophobicity of surfaces can be changed by coatings. Figure 4.2 shows a comparison between the surface roughness of ice formed on a bare graphite and a methanol coated graphite at the same surface temperature (185 K). In the upper panel, water was deposited on the bare graphite surface, and the light intensity was diminished during the ice growth indicating the formation of 3D structures. In the

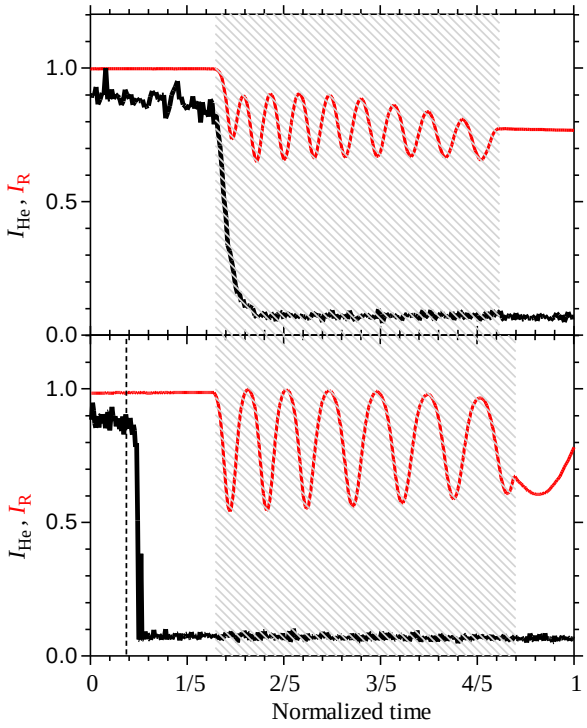

Figure 4.2 Ice formation on bare graphite surface and methanol coated graphite surface at 185 K: I_{He} and I_R as a function of normalized time. The methanol source was opened as the dashed line indicates, and kept open in the whole experiment. The shaded areas indicate the time periods that the water source was switched on. See Paper II for further details.

lower panel, the dashed line indicates when the methanol valve was opened. The helium scattering indicates that the graphite surface was rapidly covered by a thin methanol film. The wetting of methanol on graphite originates from the fact that the combination of methanol-graphite and methanol-methanol interactions makes the 2D structure stable[79-81]. Subsequently, when water vapor was inlet a macroscopically thick ice layer was formed with a smooth surface, as determined by the unattenuated light interference pattern. Furthermore, even a small fraction of methanol coverage on graphite was observed to have a strong effect on smoothening ice surface morphology. Figure 4.3 compares the light attenuation from ice formed on surfaces with initially different methanol coverages. On bare graphite, the impinging water molecules will leave the surface rapidly if they cannot find other water molecules or clusters, resulting in the 3D structures. The effect is amplified at high temperatures, where time scales for relaxation are short. Methanol molecules are attracted to both the graphite and the water, which allows the methanol to act as an intermediary and to help water spread across the surface. Thus, the hydrophobic surface can be changed to hydrophilic by a surface coating.

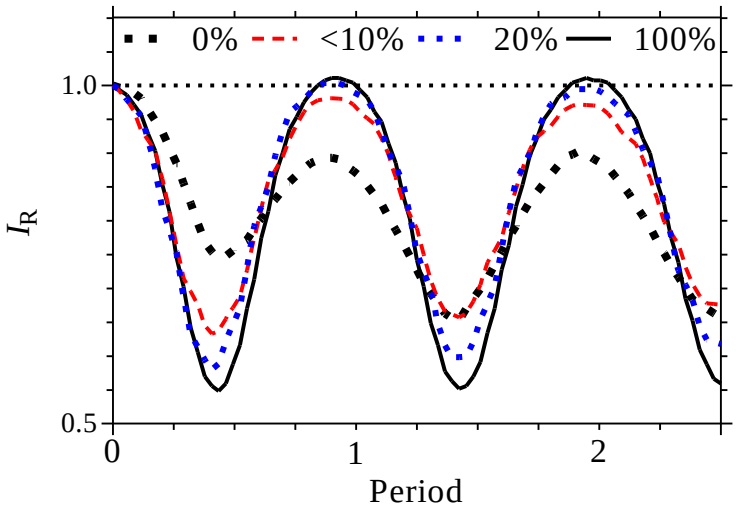

Figure 4.3 Examples of the first three I_R intensity maxima in the cases of different initial methanol coverages. See Paper II for further details.

Whether other alcohols show such a surface effect depends to some degree on the length of their carbon chains. Ethanol behaves similarly to methanol according to simulation studies[82], but butanol and hexanol layers do not alter the hydrophobicity of graphite in our experiments. These two alcohols form very robust monolayers on graphite that is significantly different from their bulk structures. Water molecules interact weakly with these monolayers and we observe very short residence times for water molecules impinging on butanol and hexanol layers regardless of temperatures. Obviously, the length of the alkyl tails and resulting layer structure play a direct role in the hydrophobicity of the alcohol layers.

4.1.3 Critical supersaturation ratio for ice nucleation

From the perspective of atmospheric research, an important parameter is the critical supersaturation (S_i) that is defined as the ratio of the pressure required for nucleation to occur divided by the equilibrium pressure over ice at the same temperature. This ratio partially determines the formation of ice particles in the atmosphere, but its values from experimental results and field measurement data are still largely unconstrained[23]. Using the EMB method, we conducted a series of deposition nucleation experiments on various surfaces at temperatures ≤ 200 K. The results of S_i are shown in Figure 4.4. The black points indicate the S_i required for deposition nucleation on bare graphite, while the other symbols correspond to ice nucleation on other monolayer materials on graphite. The solid line is the theoretical water saturation[83], and the dashed line is the theoretical supersaturation ratio for homogeneous ice nucleation[84]. In all cases, the required S_i increases dramatically with decreasing temperature and is surprisingly higher than the theoretical predictions. However, some earlier studies carried out at low temperatures also find evidences that S_i begins to increase at low temperatures in field measurements[20,21,29,30] and laboratory studies[85,86].

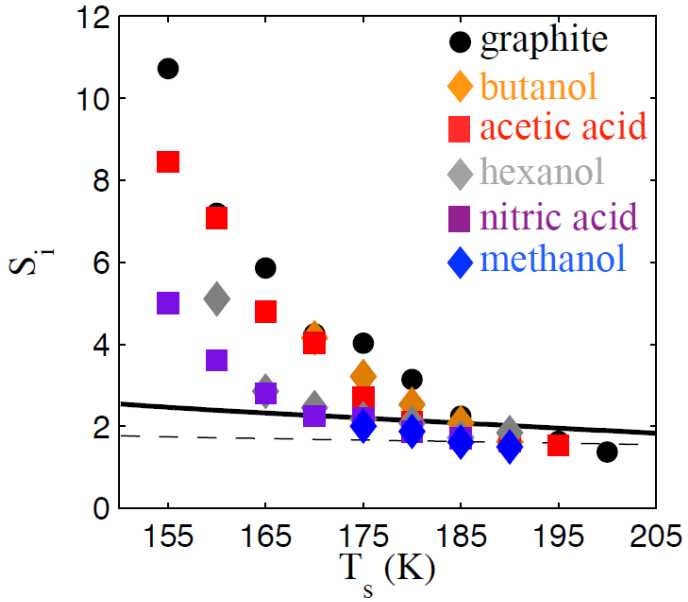

Figure 4.4 Critical supersaturation ratio (S_i) for water deposition freezing on various surfaces including bare graphite and graphite with monolayers of the compounds indicated in the panel. The solid line is theoretical curve for pure water saturation, and the dashed line is theoretical supersaturation ratio for homogeneous ice nucleation. See Paper III for further details.

The variation between different cases originates from the behavior of water on the different surfaces. Graphite is a hydrophobic surface, on which it is difficult for water to form ice embryos; while methanol and nitric acid are relatively hydrophilic, thus the required S_i values are substantially lower.

Nucleation is essentially a statistical thermodynamics process, the occurrence of nucleation is described by a nucleation rate J (s^{-2} cm^{-2} or s^{-1} cm^{-3}), and the deposition nucleation rate can be written as,

$$J = \varphi\beta Z N_{ads} \exp\left(\frac{-\Delta G^*}{k_b T} \times f\right) \quad (5)$$

where β is the impingement rate of gas molecules onto the nucleus; Z is the Zeldovich factor, describing the probability of the critical nuclei growing to reach stable size; N_{ads} is the number of adsorbed molecules on the surface; φ represents additional kinetic factors, ΔG^* is energy barrier to form a critical nucleus, k_b is the Boltzmann's constant, T is the temperature, and f is a geometry correction factor. Giving J = 1 s^{-2} cm^{-2}, which is a commonly used value in previous theoretical studies, Equation (5) can be used to fit our experimental data. Figure 4.5 shows two example fitting results for bare graphite and nitric acid coated graphite. By looking into all the parameters in the equation (see Paper III), S_i is largely determined by the binding energy of water to the surfaces and also the geometrical property of the water cluster on the surfaces.

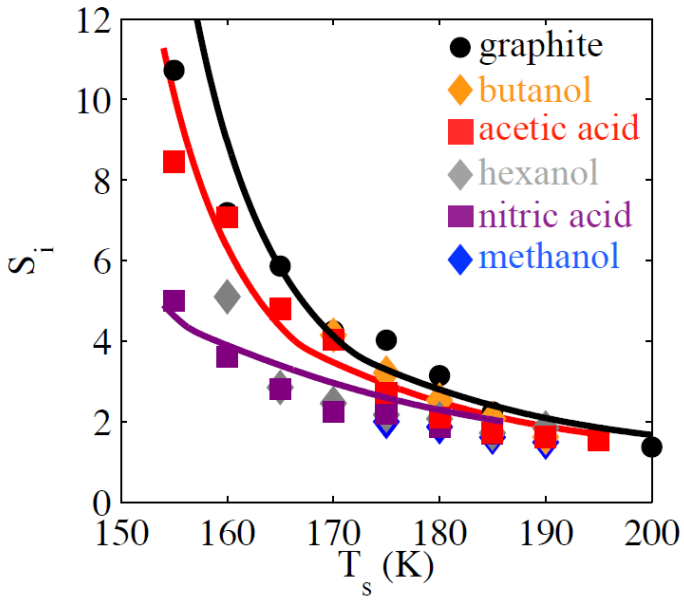

Figure 4.5 Least squares fits of theoretical values to two extreme measured dataset. The black curve is for graphite, the red is for acetic acid and the purple is for nitric acid. See Paper III for further details.

4.2 Water uptake by bare ice and coated ice

Ice particle growth influences the life time and properties of clouds, and thereby impacts the radiation budget of the Earth. Given a known water vapor pressure, it is well-established how to estimate the collision rate of gas phase molecules with a surface. However, only part of those colliding molecules contributes to ice particle growth, while others quickly re-escape from the surface. The fraction of the incoming molecules that becomes incorporated into the condensed phase is termed the accommodation coefficient (α). This parameter dramatically varies from study to

study, introducing significant uncertainty into cloud models. In this section, the results for the accommodation coefficient of water on bare ice and coated ice will be discussed together with the uptake kinetics.

Accommodation of gas molecules by the condensed phase can be understood in two ways, i.e. thermal accommodation α_t and mass accommodation α_m. The thermal accommodation coefficient is defined as the proportion of the colliding molecules that become thermalized to the surface temperature[87-89]. The energy exchange between molecules takes place on the time scale of picoseconds, and thus this parameter is often studied in molecular dynamics (MD) simulations or other theoretical calculations (Figure 4.6)[87]. In terms of mass transfer, the accommodation can be divided further into surface accommodation α_s and bulk accommodation α_b[88]. The surface accommodation refers to the fast process (also picoseconds) when molecules are trapped on surfaces after collisions. Bulk accommodation occurs when molecules move from the surface into the bulk. Molecules that do not incorporate will eventually desorb from the surface. Such processes take place over longer time scales that depend on the temperature and the interactions between gas and surface molecules. For example, water molecules on ice at 200 K spend approximately 5 milliseconds before desorbing or diffusing into the bulk.

The time difference is a way to distinguish α_s and α_b. The EMB method has the advantage of obtaining TOF distributions with high time resolution, which covers water's the residence time of water on ice (τ_w) above 170 K (Figure 4.6).

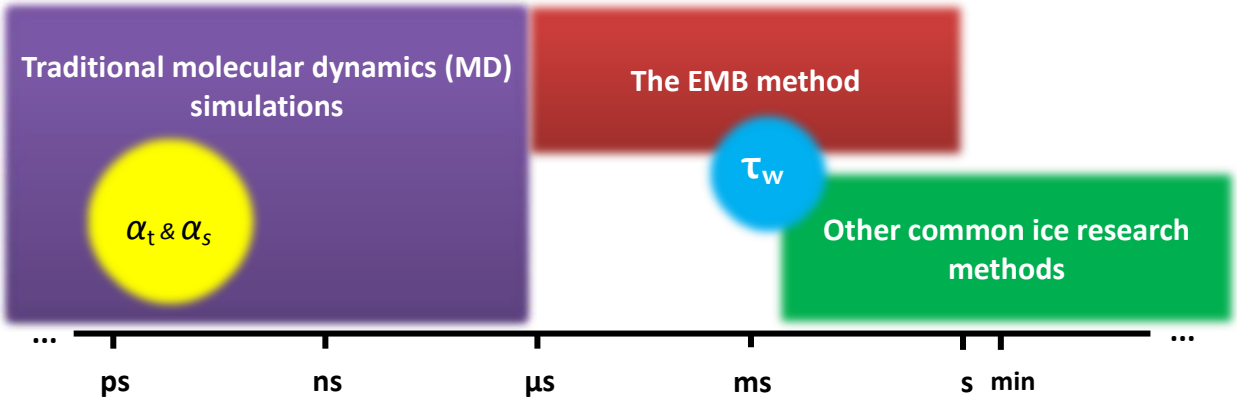

Figure 4.6 Illustration of the time resolution of simulation and experimental studies of ice.

4.2.1 Water uptake by bare ice

4.2.1.1 Kinetic models

Kinetic information concerning water adsorption and desorption on various surfaces can be extracted from time-of-flight data. Figure 4.7 illustrates typical TOF data for D_2O desorbing from bare ice. The distribution can be fitted by a first-order exponential decay as shown by the black curve. Because no inelastic scattering

component is observed, all beam molecules were assumed to be trapped on the ice surface. Hence, the thermal accommodation coefficient α_t and the surface accommodation coefficient α_s are both unity. In this case the impinging D_2O molecules were accelerated by helium atoms to have a high kinetic energy of 31 ± 2 kJ/mol (thermal velocity at 3730 K), and the lack of inelastic scattering indicates that energy exchange between the water molecule and the ice surface is very efficient.

According to Equation (3), the decay rate constant, k, was determined by the non-linear least squares fitting algorithm. Depending on the precise kinetic model, k can be interpreted as a rate constant corresponding to different processes. Applying a one-stage kinetic model,

$$D_2O\ (gas) \underset{k_{des}}{\overset{k_{ads}}{\rightleftharpoons}} D_2O\ (solid)\ , \qquad (6)$$

where D_2O (gas) is D_2O molecules in the gas phase and D_2O (solid) is water ice; k_{ads} and k_{des} are the adsorption and desorption rate constants, respectively. In experiments, all D_2O molecules were adsorbed on the ice surface by a short gas pulse,

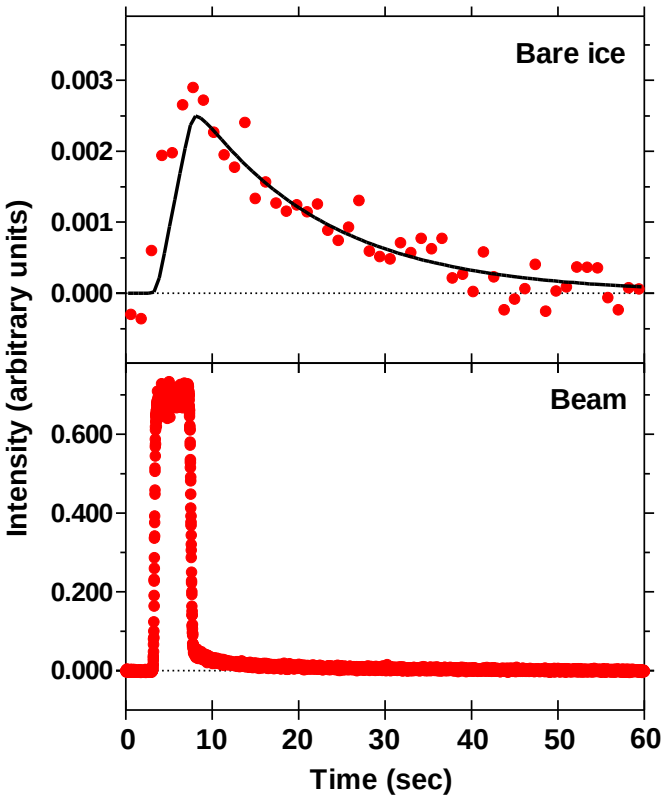

Figure 4.7 Time-of-flight distributions for D_2O desorbed from a bare ice surface at 190 K. The red points are experimental data. The black curve is the non-linear least squares fitting to the data. An incident beam profile is shown in the lower panel. See Paper IV for further details.

thus no adsorption takes place during the following desorption. Thus k_{des} is the measured k, and using an Arrhenius plot (Figure 4.8) a desorption activation energy of 17.7 ± 4.1 kJ mol^{-1} and a pre-exponential factor $A = 1 \cdot 10^{(7 \pm 1)}$ s^{-1} are obtained. This activation energy is low compared to the sublimation enthalpy of ice (54.0 ± 4.2 kJ mol^{-1})[90]. However, as described below the single stage model does not capture the true kinetics including both desorption and accommodation. Pratte *et al.*[91] reported similar findings and identified a change in kinetics at a 'break' temperature of around 190 K.

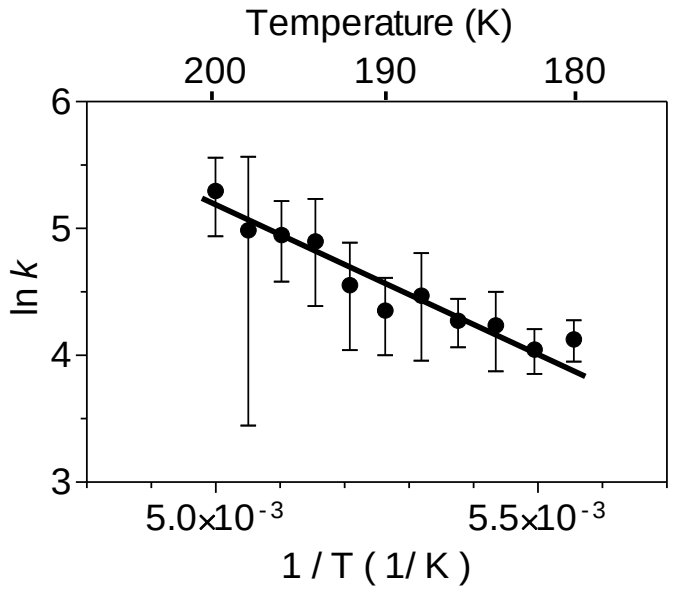

Figure 4.8 Arrhenius plot of the rate constant k for D_2O emission from ice. The solid line is a least-squares fit to the data. Error limits are 95% confidence intervals from fits to individual TOF distributions.

Alternatively, a two-stage precursor model can be used to interpret the experimental data,

$$D_2O(gas) \underset{k_{des}}{\overset{k_{ads}}{\rightleftharpoons}} D_2O(p) \underset{k_{-1}}{\overset{k_1}{\rightleftharpoons}} D_2O(solid) \qquad (7)$$

Here $D_2O(p)$ is a precursor state, k_1 is the rate constant for transfer to a strongly bound state and k_{-1} is the rate constant for the reverse process. Adsorption can again be ignored since no adsorption takes place after the initial gas pulse, and the process with rate constant k_{-1} is considered to be negligible since the measured data are well described by a single exponential decay. The intensity of measured flux is proportional to the population of $D_2O(p)$, which is governed by both k_{des} and k_1. The rate equation can be written as,

$$\frac{d[D_2O(p)]}{dt} = -k_{des}[D_2O(p)] - k_1[D_2O(p)] = -(k_{des} + k_1)[D_2O(p)] \qquad (8)$$

Thus, the measured decay rate constant k is equal to the sum of k_{des} and k_1,

$$k_{obs} = k_{des} + k_1 \,, \tag{9}$$

The bulk accommodation coefficient α_b can also be expressed by k_{des} and k_1 because it is the ratio of incorporated molecules compared to the total number of molecules,

$$\alpha_b = k_1/(k_{des} + k_1) \,, \tag{10}$$

Using Equations (9) and (10), k_{obs} and α_b were fitted simultaneously by k_{des} and k_1 in a non-linear least squares fashion. Figure 4.9 shows the measured data, the overall fitting, and the fitted k_{des} and k_1 in an Arrhenius plot, where the desorption activation energy from the precursor state is E_{des} = 42 ± 8 kJ mol^{-1} with a pre-exponential factor A_{des} = 1·10$^{(13.1 \pm 2.1)}$ s^{-1}. The pre-exponential factor agrees well with an ordinary first order desorption process, and the calculated E_{des} implies that on average newly adsorbed water molecules form more than one hydrogen bond with other surface water molecules. This finding also agrees with other studies covering the same temperature range[91-94].

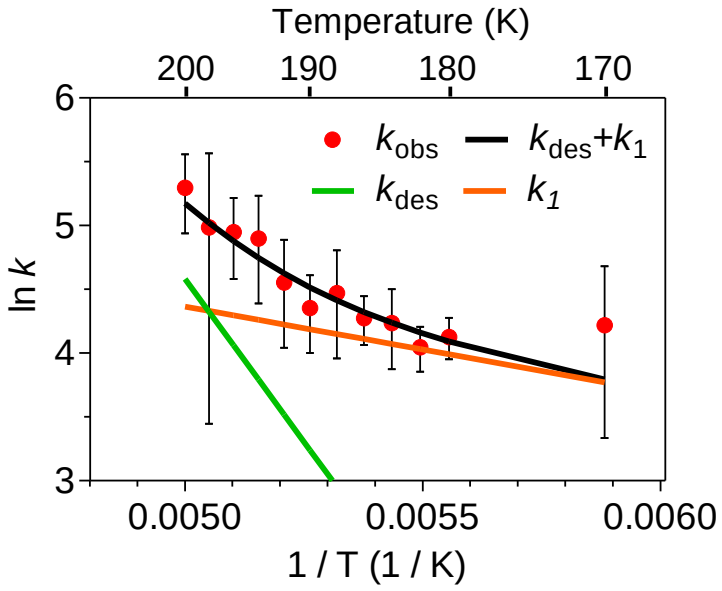

Figure 4.9 Arrhenius plot of the experimentally observed rate constant k_{obs} for D_2O emission from ice (red points), and the precursor model fit to the data (black line). The deconvoluted components k_{des} (green line) and k_1 (orange line) are also plotted. Error bars represent the 95% confidence intervals obtained from fitting individual TOF distributions. See Paper IV for further details.

4.2.1.2 Bulk accommodation coefficient

Figure 4.10 plots the bulk accommodation coefficient from our work together with literature data. Our measured α_b decreases with temperature from nearly unity at 170 K to 0.41 ± 0.20 at 200 K, which is comparable to or higher than other results. The studies using molecular beam techniques (red symbols) consistently show high

values over the temperature range of the figure. The negative temperature dependence matches the overall trend of all the collected data, which can be explained by the precursor model. The black curve in the inset panel is the result from the fitting based on Equation (10), and the grey shading is the estimated uncertainty based on the 95% confidence intervals of calculated activation energies and pre-exponential factors.

Assuming that the precursor model is still valid at higher temperatures, E_{des} and A can be used to extrapolate α. For instance, α_b decreases to $0.096^{+0.061}_{-0.039}$ at 220 K the value is $0.019^{+0.010}_{-0.007}$ at 240 K. However, as the temperature approaches the melting point, the ice surface condition may change significantly due to the presence of a QLL[95]. New EMB measurements at higher temperatures would be beneficial in the future.

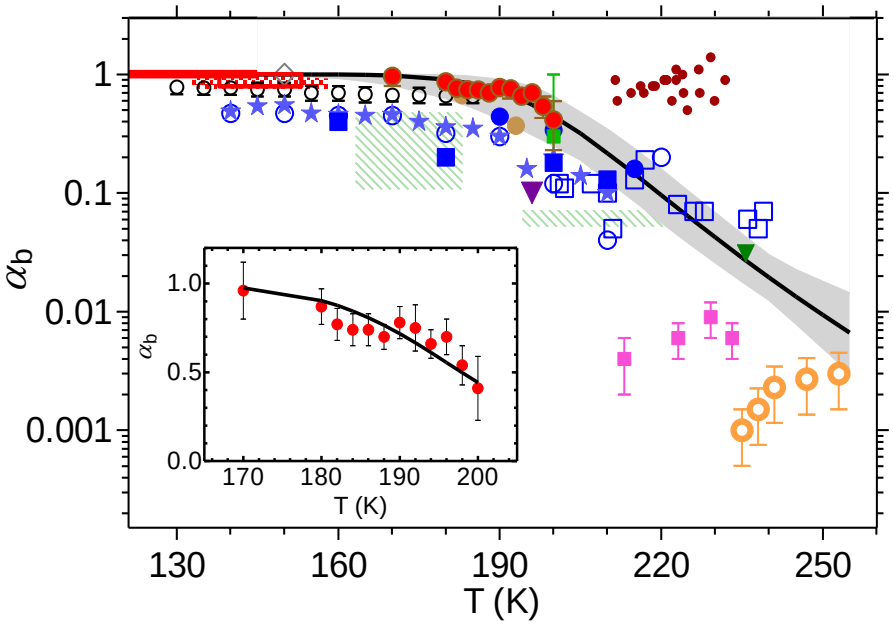

Figure 4.10 The accommodation coefficients for D_2O on water ice from the present study and comparison with literature values for the H_2O-ice system; this study ( ); Koros *et al.*[60] ( ); Brown *et al.*[58] ( ); Bryson *et al.*[59] ( ); Tolbert and Middlebrook[96] ( ); Davis and Strickland-Constable[97] ( ); Haynes *et al.*[98] ( ); Fluckiger and Rossi[93] ( ); Leu[99] ( ); Kramers and Stemerding[100] ( ); Delval *et al.*[101] ( ); Delval and Rossi[92] ( ); Pratte *et al*[91]. ( ); Chaix *et al.*[102] ( ); Isono and Iwai[103] ( ); Earle *et al.*[104] ( ); Magee *et al.*[105] ( );Choularton and Latham[106] ( ). The black line is a fit to the present experimental data using Equation (10) and an extrapolation to higher temperatures. The grey area indicates 95% confidence intervals. See Paper IV for further details.

4.2.2 Coating effects

Heterogeneous compounds can usually not incorporate into the ice lattice, and instead tend to concentrate on ice surfaces or in grain boundaries. Hence, surface

processes, such as uptake of gas molecules, are potentially influenced by the presence of impurities. Figure 4.11 shows the water accommodation coefficients on various coated ice surfaces compared to the bare ice. Both acetic acid and nitric acid are abundant in the troposphere, and are easily taken up by ice particles[45,107], and the α_b values are enhanced to unity by the presence of these two acidic coating.

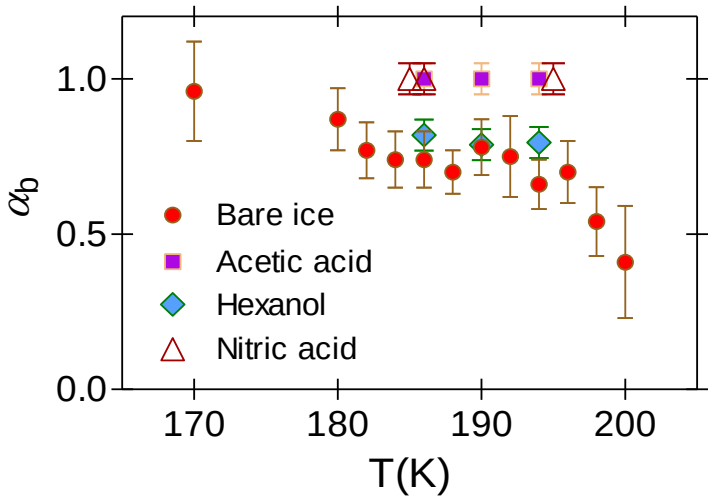

Figure 4.11 Water bulk accommodation coefficient on nitric acid-covered ice (△), *n*-hexanol-covered ice (◇), acetic acid-covered ice (■) and bare ice (●). See Paper IX for further details.

Compared to the bare ice, hexanol coatings do not have a major impact on the accommodation coefficient, but they alter the desorption kinetics, which can be seen by comparing the peak shapes in the two distributions shown in Figure 4.12. The accommodation coefficient is related to the area of the desorption peak, regardless of the peak shape, i.e. the desorption rate constant is not considered. Note that the peak of bare ice has been amplified by a factor of 20 in order to be visible together with the hexanol data. From the hexanol coated ice, some of the impinging molecules were inelastically scattered, and some of the trapped molecules desorb rapidly with a residence time below 20 μs. To understand these fast processes in detail, MD simulations are a helpful approach that can be used for further investigations.

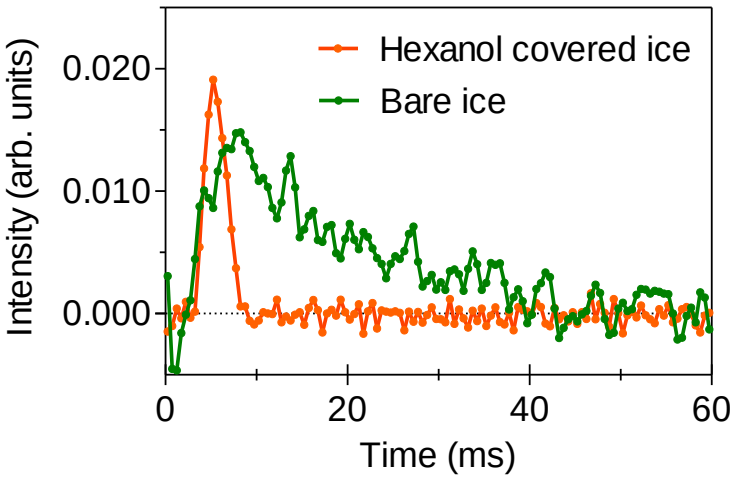

Figure 4.12 TOF distributions for D_2O emitted from bare ice and hexanol coated ice surfaces at 190 K. See Paper IX for further details.

In Figure 4.13, the α_b values were determined on a relative short time scale of 10 ms instead of 60 ms that was used for Figure 4.11. The hexanol, acetic acid and nitric acid data are identical to those shown in Figure 4.11 because the desorption is fully captured in 10 ms. The methanol coating does not significantly impact water uptake compared to bare ice; while butanol reduces water uptake by approximately 20%.

Methanol is the smallest alcohol and the second most common organic compound in the atmosphere after methane. The only difference between methanol and water molecules in structure is the exchange of a methyl group for a hydrogen atom, and this similarity in their structures makes their interactions with water distinctive[80]. On the other hand, adsorbed butanol could hinder water due to its larger size and hydrophobicity. Alcohols containing more than 14 carbon atoms are known to substantially reduce water evaporation, and the effectiveness shows a positive correlation with the alkyl length[108,109]. Using molecular dynamics (MD) simulations, Gilde *et al.*[110] reported that a butanol monolayer decreases water condensation on

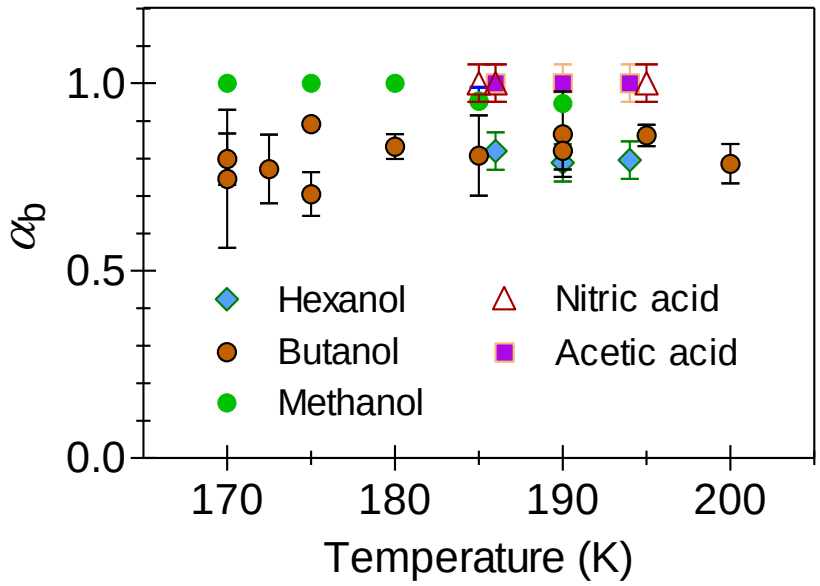

Figure 4.13 Water bulk accommodation coefficient on ice coated with different adsorbates: nitric acid (△), acetic acid (■), hexanol (◆), butanol (●) and methanol (●). The experimental time scale is 10 ms, compared to 60 ms that was used in Figure 4.11. See Paper IX for further details.

liquid water by a factor of about 3 compared to bare ice. In contrast, Nathanson *et al.*[111] have shown butanol monolayers to have little effect on D_2O evaporation from super-cooled sulfuric acid using a molecular beam technique. In the time scales of MD simulations, water has little chance to escape from ice, but a higher probably to desorb from coated ice surfaces. Thus, the findings of Gilde and Nathanson indicate that butanol coatings might behave similarly to that of hexanol, changing the desorption kinetics but having a minor impact on accommodation coefficients.

Overall, in this section the desorption kinetics and accommodation coefficients of water on bare ice have been elaborated. The experimental data from bare ice can be quantitatively fitted by a precursor model, which also predicts the α_b values at higher temperatures. When the ice surface is coated by acidic compounds, acetic acid and nitric acid, the α_b values are enhanced to unity. Hexanol coatings do not influence α_b but alter the desorption kinetics compared to bare ice. On a short time scale, methanol coatings do not have a significant effect on water uptake, while butanol reduces α_b by 20%. The length of the alkyl tails of coating alcohols seems to play a role on decreasing ice sublimation and water evaporation rates.

4.3 Water interactions with organic surfaces

Organics coat aerosol particles and form organics aerosols, thus the formation and the surface properties of organic coatings on aerosol surfaces are of interest due to their atmospheric implication. The interaction of water with organic surfaces is also

an interesting fundamental topic, and in this section EMB studies of thin adsorbed organic layers on graphite and macroscopic organic phases are discussed.

4.3.1 Thin organic coatings on graphite

The methanol film on graphite is found to alter the surface hydrophobicity as discussed in section 4.1.2. Figure 4.14 shows a series of TOF distributions for water interactions with various coatings on graphite. Except for methanol, on the other three coatings water spends too short time (< 20 μs) to be characterized with the current EMB time resolution. The butanol, hexanol and acetic acid films are relatively easy to form on the graphite compared to building up their bulk phases, and the adlayers are rather stable and significant annealing is required to evaporate them from the graphite.

The methanol film is studied in detail in the temperature range from 175 K to 190 K. Because the melting point of the methanol monolayer is 135 K, the investigated methanol film here should be liquid-like. Figure 4.15 shows the temperature dependence of the rate constants of water desorption from the methanol film in Arrhenius style. The calculated Arrhenius parameters are an activation energy E_A = 0.47 ± 0.11 eV and a pre-exponential factor $A = 4.6\times10^{(15\pm3)}$ s $^{-1}$. According to the E_A value, water molecules form approximately two hydrogen bonds with the methanol adlayer.

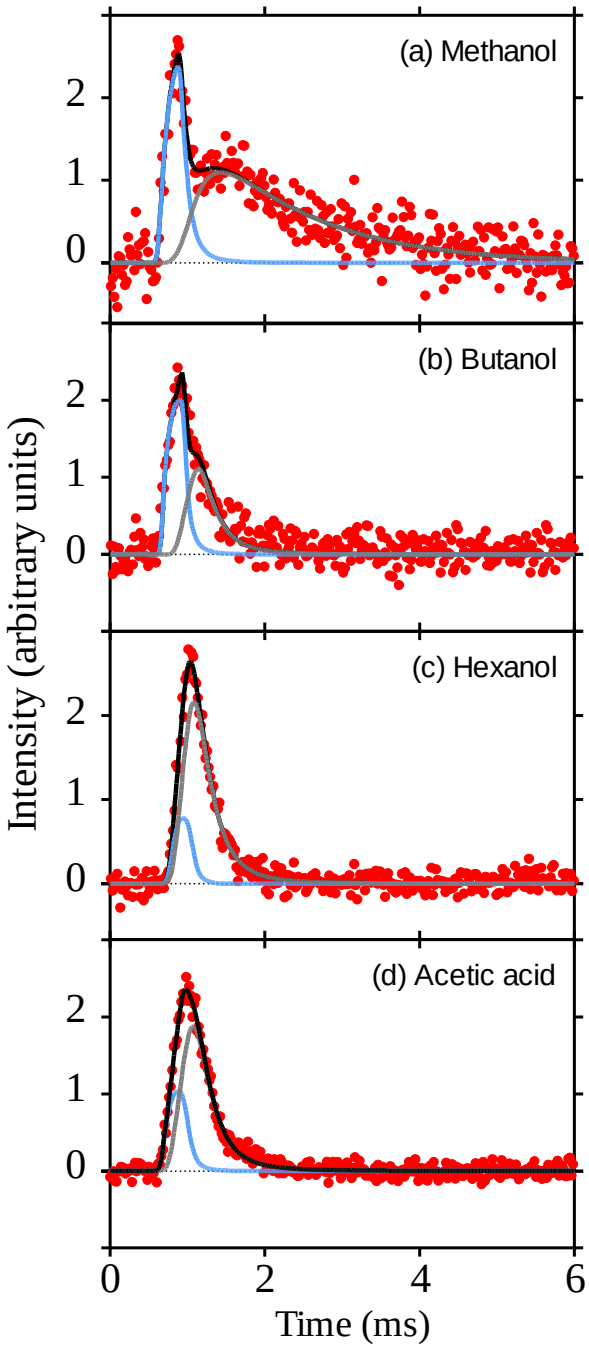

Figure 4.14 Time-of-flight distributions for D_2O inelastic scattering and thermal desorption from (a) a methanol film, (b) a butanol film, (c) a hexanol film, and (d) an acetic acid film on graphite. The surface temperatures are 185 K in (a), (b), and 190 K in (c), (d). The grey, black and blue curves show the total, inelastic and thermal desorption components, respectively.

The solvation of water molecules in the methanol film is illustrated in Figure 4.16, where the fraction of trapping-desorbed D_2O molecules is plotted as a function of temperatures. The TD fraction increases with temperatures. Below 180 K only 20-30% of the trapped D_2O molecules desorbs again on the time scale of the experiment,

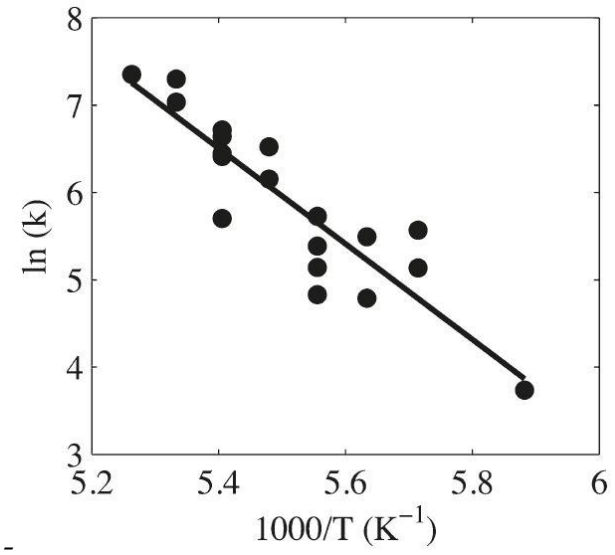

Figure 4.15 Arrhenius plot of the rate constants for desorption of D_2O from liquid methanol. The solid line is a linear least-squares fit to the data. See Paper V for further details.

while at 190 K almost all D_2O leaves within 10 ms. The trapped D_2O molecules could be incorporated into the methanol film, which complies with the finding that the adsorbed methanol film makes the graphite surface hydrophilic.

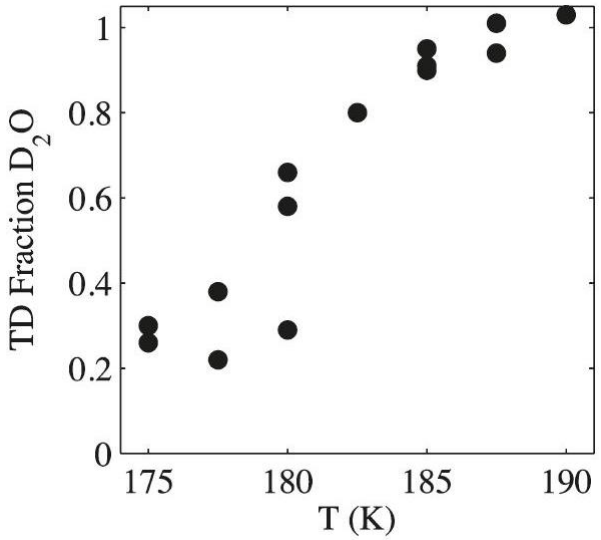

Figure 4.16 The fraction of trapped and thermally desorbed D_2O molecules on liquid methanol as a function of temperature. See Paper V for further details.

The formation of organic coating plays an important role in atmospheric research, and thus their adsorption and desorption isotherms are of interest. Figure 4.17 shows an example isotherm of acetic acid adsorption and desorption on graphite at 190 K. The surface coverage increases with acetic acid vapor pressure and a complete monolayer is formed when the relative vapor pressure is approximately 0.17. When decreasing the pressure, a hysteresis effect is observed and the coverage does not begin to decrease until the relative vapor saturation is below 0.05. This can be

classified as a Type V isotherm according to Brunauer *et al.*[112], indicating strong intermolecular interactions.

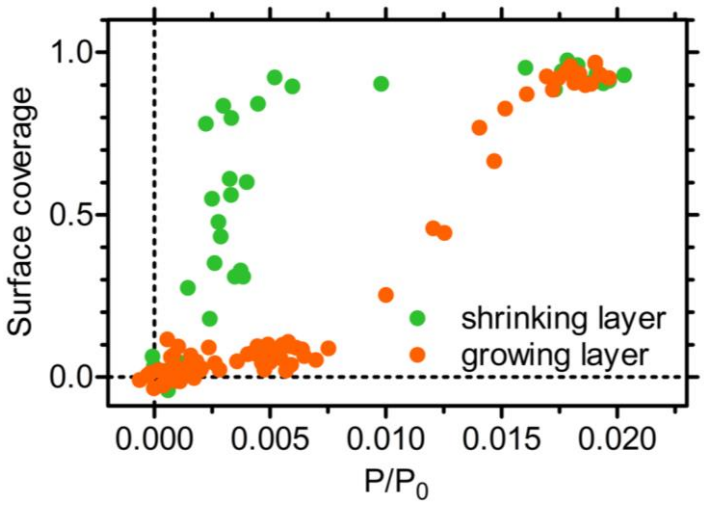

Figure 4.17 Sub-monolayer surface coverage of acetic acid on graphite as a function of acetic acid pressure during layer growth (orange) and shrinkage (green). The surface temperature was 190 K. See Paper VI for further details.

4.3.2 Bulk organics

The interactions of water and the surfaces of butanol, hexanol and acetic acid bulks phases have been studied, and Figure 4.18 shows typical TOF distributions for water emission from the bulk surfaces at 190 K. Bulk butanol undergoes a phase transition between solid and liquid within the applicable pressure range of the EMB method. The surface properties and water accommodation near the bulk phase transition are discussed in the following. Such processes and parameters have been analogously discussed in another system, water on bare ice (Section 4.2.1), which motivates the connection between Paper IV and Paper VII shown in Figure 1.1.

The desorption rate constants k and water accommodation coefficients α have been calculated from the TOF data in the same way as described above. The upper panel of Figure 4.19 shows the k for D_2O desorption from butanol layers with different histories: newly formed at each temperature (orange), formed at low temperature and annealed by warming (purple), and formed at high temperature and subsequently cooled (green). In the low temperature range (< 180 K), the butanol surface is solid, and the desorption rate constant increases with increasing temperature.

When the temperatures are close to the melting point T_m, k undergoes gradual changes over a 10 K span (grey area), indicating that the surface has already started to melt 4.5 K below T_m. Furthermore, the surface is not fully liquefied until the temperature is 5.5 K above T_m. When the temperature is even higher, the desorption peak is too small to be characterized. The k values in the cooling case are lower than

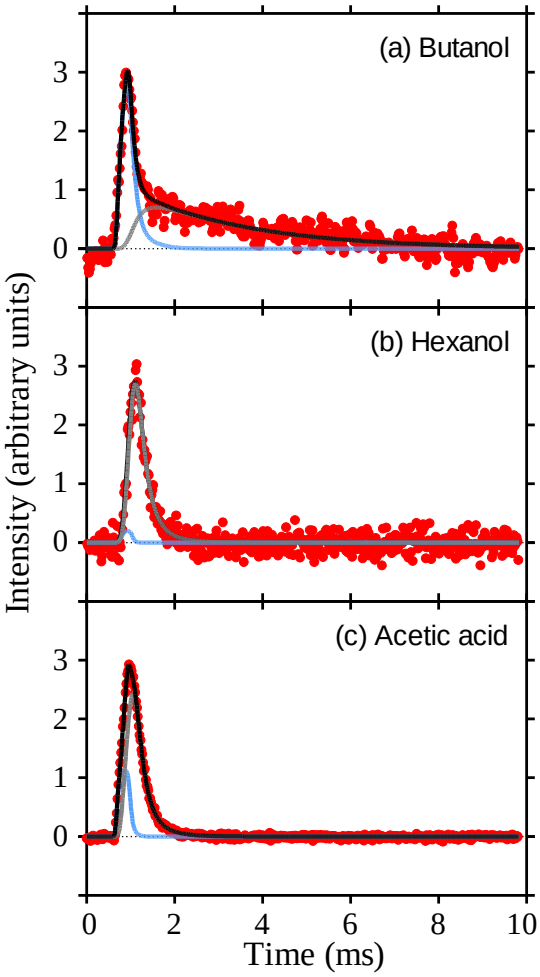

Figure 4.18 Time-of-flight distributions for D_2O inelastic scattering and thermal desorption from (a) a bulk butanol layer, (b) a bulk hexanol layer, and (c) a bulk acetic acid layer at 190 K. The black, blue and grey curves show the total, inelastic and thermal desorption components, respectively.

those in the other two cases, which indicates the butanol layer might be supercooled because a liquid surface could prolong the residence time of beam molecules.

The lower panel shows the accommodation coefficients of water on butanol surfaces. On solid butanol (< 180 K), the α_b values decrease with temperature, which is qualitatively similar to the negative temperature dependence for water accommodation on solid ice shown in Figure 4.10. When surface melting occurs around T_m, the uptake becomes gradually more efficient, which could be due to the increasing disordering and depth of the surface layers. At temperatures above 190 K, the butanol layer fully melts, and the α_b turns to very high values, analogous to high water accommodation coefficients on liquid water[113].

In summary, the organic coatings on graphite have various properties. Butanol, hexanol and acetic acid form stable films with which water molecules interact weakly. The liquid-like methanol film shows desorption described by the Arrhenius equation at temperatures from 170 K to 190 K, and the water solvation on the film increases

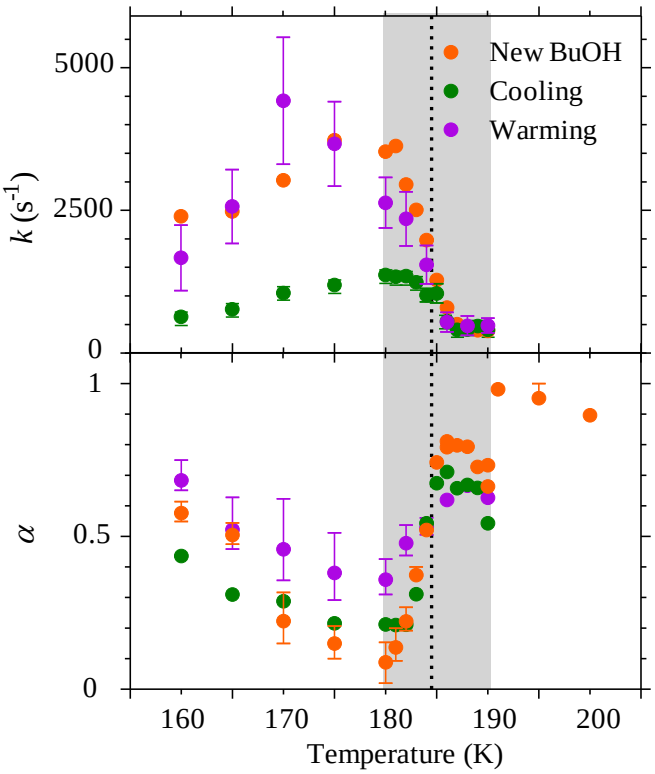

Figure 4.19 Desorption rate constant k (upper panel) and accommodation coefficient α (lower panel) for D_2O on butanol layers produced in different procedures: liquid butanol deposited at 200 K and cooled to 160 K (green), solid butanol deposited at 160 K and warmed to 190 K (purple), and new butanol layer deposited at each temperature (orange). The dotted line indicates the melting temperature T_m = 184.5 K for butanol. See Paper VII for further details.

with temperature. Bulk butanol undergoes a solid/liquid phase transition within the experimental temperature range of 160 K – 200 K, and the water desorption kinetics and accommodation coefficients gradually change during the surface phase transition within a temperature span of 10 K. The correlation between α_b and solid/liquid phase changes could be compared with water uptake on ice surfaces during ice surface premelting, which is known to occur well below the ice T_m and have significant environmental relevance.

Chapter V

Summary

This thesis describes experimental studies of atmospherically relevant interface processes, including ice formation and water interactions with ice and organic surfaces. The studies are based on the EMB method, and the design and validation of the method is described (Paper I).

The results are divided into three major parts, which are (1) Ice formation via deposition freezing, (2) Water uptake by bare ice and coated ice, and (3) Water interactions with organic surfaces. In the first part, ice formation via deposition mode nucleation on a hydrophobic surface at temperatures up to 213 K is illustrated. The surface hydrophobicity can be altered by a methanol coating, which is observed by monitoring the morphology of formed ice surfaces (Paper II), while butanol and hexanol coatings do not have such surface effects. The critical supersaturation required to activate deposition freezing on various surfaces is studied, and a dramatic negative temperature dependence is consistently observed for all surfaces at the temperatures below 200 K (Paper III).

The results of water uptake by bare ice and coated ice are discussed in three papers (IV, VIII, IX). The accommodation coefficient of water on bare ice is negatively correlated to the temperature, and the results are quantitatively described by a precursor kinetics model. Surface coatings have a significant impact on uptake processes. Acetic acid and nitric acid enhance the α_b to unity, and hexanol does not affect the α_b values on a long time scale (60 ms), but alters the desorption kinetics. On a short time scale (10 ms), methanol coatings do not influence water deposition compared to bare ice, while butanol and hexanol shorten the water residence time on the surface.

In the third part, the organic surfaces are further divided into organic coatings on graphite (Paper V, VI, IX) and bulk organic surfaces (Paper VI, VII, IX). Bulk accommodation is inefficient on solid alcohol and acetic acid surfaces, while water uptake is efficient on liquid organic phases including a liquid methanol monolayer on graphite and liquid butanol. The surface layer on bulk butanol also shows a gradual phase change over a temperature span of 10 K around the bulk melting temperature.

The issues covered in this thesis relate to atmospheric processes. The ice formation and critical supersaturation results contribute to the fundamental understanding of ice particle formation at low temperatures. The water accommodation results help to constrain the uncertainty in ice particle growth rates, which affects the development

of clouds and thus their effects on the climate system. The interactions between water and organic surfaces are of central importance in aerosol formation and growth, and the present studies contribute to the development of a molecular-level understanding of the processes taking place at environmental interfaces.

Acknowledgements

I owe particular thanks to my supervisor **Jan Pettersson**, who guided and influenced me in many aspects. There are so many scientific discussions and personal chats between us in the last several years, and many of them are memorable.

I am very pleased to have **Erik Thomson** as my assistant supervisor, from whom I learned many things about scientific attitude, analytical thinking, and also the language!

It is delightful to work with **Panos Papagiannakopoulos**, who is passionate and energetic to both science and life.

Many thanks to my former assistant supervisor **Patrik Andersson**, who built the base of my knowledge and skills in the laboratory.

I must record my thankfulness to the master of laboratory engineering **Benny Lönn**, who helps us to make sketches to real stuffs.

The examiner of my PhD study **Evert Ljungström** gives me many encouragements on the research and makes sure that I have good working conditions, which let me feel supported and guaranteed. Thank you!

Torbjörn Gustafsson helped me so much to begin the research in atmospheric science. Every time we talk I always learn new things.

The opportunity for me to enter this group was given by **Johan Boman**, and there are so many different kinds of helps I got from you in these years. Thank you so much!

The teaching duty gives me important experiences, so I would like to thank all the people that I worked together with in teaching, especially **Lennart Sjölin** and **Barbara Casari**.

I want to thank all the **current and former members in the Atmospheric Science group**. We know the atmosphere, and we built a good one in our group.

Friends make up parts of my life, and it is very grateful to have them.

Family is the base for everything. Thanks to my wife, **Xiaolu Zhang**, who did a lot to support me. And **Xuanxuan**, you are another treasure that I got in these years, besides this thesis.

References

1 Aristotle. *Meteorology* (350 B.C.E).

2 Stradling, G. F. Physical section - Recent advances in the physics of water. *J. Frankl. Inst.* **152**, 257-268 (1901).

3 Mpemba, E. B. & Osborne, D. G. Cool? *Phys. Educ.* **4**, 172-175, doi:10.1088/0031-9120/4/3/312 (1969).

4 Ian, F. Cooler? *Phys. Educ.* **6**, 32 (1971).

5 Rosenberg, R. Why is ice slippery? *Phys. Today* **58**, 50-55 (2005).

6 Joly, J. *Proc. R. Soc. Dublin 5*. (1887).

7 Bowden, F. P. & Hughes, T. P. The mechanism of sliding on ice and snow. *Proc. R. Soc. Lon. Series A.* **172**, 0280-0298, doi: 10.1098/rspa.1939.0104 (1939).

8 Faraday, M. *Faraday's Diary*. Vol. IV 79 (Bell and Sons, 1933).

9 Li, Y. & Somorjai, G. A. Surface premelting of ice. *J. Phys. Chem. C* **111**, 9631-9637, doi: 10.1021/Jp071102f (2007).

10 Lee, S. S. Dependence of the effect of aerosols on cirrus clouds on background vertical velocity. *Atmos. Res.* **111**, 79-89, doi:10.1016/j.atmosres.2012.03.003 (2012).

11 Liou, K. N. Influence of Cirrus Clouds on Weather and Climate Processes - a Global Perspective. *Mon. Weather Rev.* **114**, 1167-1199 (1986).

12 Baran, A. J. A review of the light scattering properties of cirrus. *J. Quant. Spectrosc. Ra. Trans.* **110**, 1239-1260, doi: 10.1016/j.jqsrt.2009.02.026 (2009).

13 Lee, S. S., Donner, L. J. & Phillips, V. T. J. Sensitivity of aerosol and cloud effects on radiation to cloud types: comparison between deep convective clouds and warm stratiform clouds over one-day period. *Atmos. Chem. Phys.* **9**, 2555-2575 (2009).

14 Baran, A. J. From the single-scattering properties of ice crystals to climate prediction: A way forward. *Atmos. Res.* **112**, 45-69, doi: 10.1016/j.atmosres.2012.04.010 (2012).

15 Zhang, Y., Macke, A. & Albers, F. Effect of crystal size spectrum and crystal shape on stratiform cirrus radiative forcing. *Atmos. Res.* **52**, 59-75 (1999).

16 Fu, Q. A new parameterization of an asymmetry factor of cirrus clouds for climate models. *J. Atmos. Sci.* **64**, 4140-4150, doi:Doi 10.1175/2007jas2289.1 (2007).

17 Lawson, R. P., Baker, B., Pilson, B. & Mo, Q. X. In situ observations of the microphysical properties of wave, cirrus, and anvil clouds. Part II: Cirrus clouds. *J. Atmos. Sci.* **63**, 3186-3203 (2006).

18 Nakaya, U. *Snow Crystals, Natural and Artifical.*, (Harvard University Press, 1954).

19 Murray, B. J. & Jensen, E. J. Homogeneous nucleation of amorphous solid water particles in the upper mesosphere. *J. Atmos. Sol-Terr. Phy.* **72**, 51-61, doi: 10.1016/j.jastp.2009.10.007 (2010).

20 Maltagliati, L. *et al.* Evidence of Water Vapor in Excess of Saturation in the Atmosphere of Mars. *Science.* **333**, 1868-1871, doi: 10.1126/science.1207957 (2011).

21 Jensen, E. J. *et al.* Ice supersaturations exceeding 100% at the cold tropical tropopause: implications for cirrus formation and dehydration. *Atmos. Chem. Phys.* **5**, 851-862 (2005).

22 Heavens, N. G. Sunshine on a Cloudy Forecast. *Science.* **333**, 1832-1833, doi: 10.1126/science.1212490 (2011).

23 Peter, T. *et al.* When dry air is too humid. *Science.* **314**, 1399, doi:10.1126/science.1135199 (2006).

24 Pruppacher, H. R. & Klett, J. D. *Microphysics of Clouds and Precipitation*. (Kluwer Academic, 1997).

25 Cantrell, W. & Heymsfield, A. Production of ice in tropospheric clouds - A review. *B. Am. Meteorol. Soc.* **86**, 795-807, doi: 10.1175/Bams-86-6-795 (2005).

26 Vali, G. Nucleation Terminology. *B. Am. Meteorol. Soc.* **66**, 1426-1427 (1985).

27 Phillips, V. T. J., DeMott, P. J. & Andronache, C. An empirical parameterization of heterogeneous ice nucleation for multiple chemical species of aerosol. *J. Atmos. Sci.* **65**, 2757-2783, doi: 10.1175/2007jas2546.1 (2008).

28 Hoose, C., Kristjansson, J. E., Chen, J. P. & Hazra, A. A Classical-Theory-Based Parameterization of Heterogeneous Ice Nucleation by Mineral Dust, Soot, and Biological Particles in a Global Climate Model. *J. Atmos. Sci.* **67**, 2483-2503, doi: 10.1175/2010jas3425.1 (2010).
29 Gao, R. S. *et al.* Evidence that nitric acid increases relative humidity in low-temperature cirrus clouds. *Science* **303**, 516-520, doi: 10.1126/science.1091255 (2004).
30 Kramer, M. *et al.* Ice supersaturations and cirrus cloud crystal numbers. *Atmos. Chem. Phys.* **9**, 3505-3522 (2009).
31 Hallquist, M. *et al.* The formation, properties and impact of secondary organic aerosol: current and emerging issues. *Atmos. Chem. Phys.* **9**, 5155-5236 (2009).
32 NASA. *Portrait of global aerosols*, <http://www.nasa.gov/multimedia/imagegallery/image_feature_2393.html#.U1-wzKhYOBI>
33 Terhune, R. W., Maker, P. D. & Savage, C. M. Optical Harmonic Generation in Calcite. *Phys. Rev. Lett.* **8**, 404-406, doi: 10.1103/PhysRevLett.8.404 (1962).
34 Shen, Y. R. Surface-Properties Probed by 2nd-Harmonic and Sum-Frequency Generation. *Nature* **337**, 519-525, doi: 10.1038/337519a0 (1989).
35 Zhao, R. Q., Jin, K. J., Guo, H. Z., Lu, H. B. & Yang, G. Z. A study on surface symmetry and interfacial enhancement of $SrTiO_3$ by second harmonic generation. *Sci. China Phys. Mech.* **56**, 2370-2376, doi: 10.1007/s11433-013-5349-1 (2013).
36 Furukawa, Y., Yamamoto, M. & Kuroda, T. Ellipsometric Study of the Transition Layer on the Surface of an Ice Crystal. *J. Cryst. Growth.* **82**, 665-677 (1987).
37 Elbaum, M., Lipson, S. G. & Dash, J. G. Optical Study of Surface Melting on Ice. *J. Cryst. Growth* **129**, 491-505, doi: 10.1016/0022-0248(93)90483-D (1993).
38 Beaglehole, D. & Nason, D. Transition Layer on the Surface on Ice. *Surf. Sci.* **96**, 357-363, doi: 10.1016/0039-6028(80)90313-1 (1980).
39 Xue, X., He, Z. Z. & Liu, J. Detection of water-ice phase transition based on Raman spectrum. *J. Raman Spectrosc.* **44**, 1045-1048, doi:Doi 10.1002/Jrs.4310 (2013).
40 Walrafen, G. E. Raman Spectral Studies of Water Structure. *J. Chem. Phys.* **40**, 3249, doi: 10.1063/1.1724992 (1964).
41 Loubeyre, P., LeToullec, R., Wolanin, E., Hanfland, M. & Husermann, D. Modulated phases and proton centring in ice observed by X-ray diffraction up to 170 GPa. *Nature* **397**, 503-506, doi: 10.1038/17300 (1999).
42 Bluhm, H., Ogletree, D. F., Fadley, C. S., Hussain, Z. & Salmeron, N. The premelting of ice studied with photoelectron spectroscopy. *J. Phys. Condens. Mat.* **14**, L227-L233, doi: 10.1088/0953-8984/14/8/108 (2002).
43 Starr, D. E., Liu, Z., Havecker, M., Knop-Gericke, A. & Bluhm, H. Investigation of solid/vapor interfaces using ambient pressure X-ray photoelectron spectroscopy. *Chem. Soc. Rev.* **42**, 5833-5857, doi: 10.1039/C3cs60057b (2013).
44 Myneni, S. *et al.* Spectroscopic probing of local hydrogen-bonding structures in liquid water. *J. Phys. Condens. Mat.* **14**, L213-L219, doi: 10.1088/0953-8984/14/8/106 (2002).
45 Krepelova, A., Bartels-Rausch, T., Brown, M. A., Bluhm, H. & Ammann, M. Adsorption of Acetic Acid on Ice Studied by Ambient-Pressure XPS and Partial-Electron-Yield NEXAFS Spectroscopy at 230-240 K. *J. Phys. Chem. A* **117**, 401-409, doi: 10.1021/Jp3102332 (2013).
46 Krepelova, A., Newberg, J. T., Huthwelker, T., Bluhm, H. & Ammann, M. The nature of nitrate at the ice surface studied by XPS and NEXAFS. *Phys. Chem. Chem. Phys.* **12**, 8870-8880, doi:10.1039/c0cp00359j (2010).
47 Pfalzgraff, W. C., Hulscher, R. M. & Neshyba, S. P. Scanning electron microscopy and molecular dynamics of surfaces of growing and ablating hexagonal ice crystals. *Atmos. Chem. Phys.* **10**, 2927-2935 (2010).
48 Thurmer, K. & Bartelt, N. C. Growth of multilayer ice films and the formation of cubic ice imaged with STM. *Phys. Rev. B* **77**, doi: 10.1103/Physrevb.77.195425 (2008).
49 Danilatos, G. D. Foundations of Environmental Scanning Electron-Microscopy. *Adv. Electron El. Phys.* **71**, 109-250 (1988).
50 Wollan, E. O., Davidson, W. L. & Shull, C. G. Neutron Diffraction Study of the Structure of Ice. *Phys. Rev.* **75**, 1348-1352, doi: 10.1103/PhysRev.75.1348 (1949).

51 Muller-Buschbaum, P. Grazing incidence small-angle neutron scattering: challenges and possibilities. *Polym. J.* **45**, 34-42, doi: 10.1038/Pj.2012.190 (2013).
52 Stern, O. The conversion of atoms in radiation. *Z. Phys. Chem. Stoch. Ve.* **120**, 60-62 (1926).
53 Nobelprize. *The Nobel Prize in Chemistry 1986*, <http://www.nobelprize.org/nobel_prizes/chemistry/laureates/1986>
54 Lejonthun, L. S. E. R., Andersson, P. U., Nagard, M. B. & Pettersson, J. B. C. Chlorine interactions with water ice studied by molecular beam techniques. *J. Phys. Chem. B* **110**, 23497-23501, doi: 10.1021/Jp065656e (2006).
55 Alexander, W. A., Wiens, J. P., Minton, T. K. & Nathanson, G. M. Reactions of Solvated Electrons Initiated by Sodium Atom Ionization at the Vacuum-Liquid Interface. *Science* **335**, 1072-1075, doi: 10.1126/science.1215956 (2012).
56 Lee, Y. T., Mcdonald, J. D., Lebreton, P. R. & Herschba.Dr. Molecular Beam Reactive Scattering Apparatus with Electron Bombardment Detector. *Rev. Sci. Instrum.* **40**, 1402, doi: 10.1063/1.1683809 (1969).
57 Lengyel, J. *et al.* Uptake of atmospheric molecules by ice nanoparticles: Pickup cross sections. *Journal of Chemical Physics* **137**, doi: 10.1063/1.4733987 (2012).
58 Brown, D. E. *et al.* H_2O condensation coefficient and refractive index for vapor-deposited ice from molecular beam and optical interference measurements. *J. Phys. Chem.* **100**, 4988-4995 (1996).
59 Bryson, C. E., Cazcarra, V. & Levenson, L. L. Condensation Coefficient Measurements of H_2O, N_2O, and CO_2. *J. Vac. Sci. Technol.* **11**, 411-416, doi: 10.1116/1.1318639 (1974).
60 Koros, R. M., Deckers, J. M., Andres, R. P. & Boudart, M. Sticking Probability of Water on Ice. *Chem. Eng. Sci.* **21**, 941, doi: 10.1016/0009-2509(66)85088-1 (1966).
61 Kong, X., Andersson, P. U., Markovic, N. & Pettersson, J. B. C. in *12th International Conference on the Physics and Chemistry of Ice (PCI-2010).* (eds Y. Furukawa, G. Sazaki, T. Uchida, & N. Watanabe) 79-88 (Hokkaido University Press).
62 Kong, X. R., Andersson, P. U., Thomson, E. S. & Pettersson, J. B. C. Ice Formation via Deposition Mode Nucleation on Bare and Alcohol-Covered Graphite Surfaces. *J. Phys. Chem. C* **116**, 8964-8974, doi: 10.1021/Jp212235p (2012).
63 Bird, G. A. *Molecular Gas Dynamics and the Direct Simulation of Gas Flows*. (Clarendon Press, 1994).
64 Computer code DS3V, version 2. 6. 03 v. 2. 6. 03 (2008a).
65 Computer code DS2V, version 4. 5. 06 v. 4. 5. 06 (2008b).
66 Farias, D. & Rieder, K. H. Atomic beam diffraction from solid surfaces. *Rep. Prog. Phys.* **61**, 1575-1664 (1998).
67 Comsa, G. & Poelsema, B. *Atomic and Molecular Beam Methods*. Vol. 2 463 (Oxford University Press, 1992).
68 Buttner, R. & Maurer, G. B. B. Dimerisierung einiger organischer Sauren in der Gasphase. *Ges. Phys. Chem. Chem. Phys.*, 877–882 (1983).
69 Andersson, P. U., Nagard, M. B., Bolton, K., Svanberg, M. & Pettersson, J. B. C. Dynamics of argon collisions with water ice: Molecular beam experiments and molecular dynamics simulations. *J. Phys. Chem. A* **104**, 2681-2688 (2000).
70 Andersson, P. U., Suter, M. T., Markovic, N. & Pettersson, J. B. C. Water condensation on graphite studied by elastic helium scattering and molecular dynamics Simulations. *J. Phys. Chem. C* **111**, 15258-15266, doi:10.1021/jp068984n (2007).
71 Lide, D. R. *CRC handbook of chemistry and physics: a ready-reference book of chemical and physical data*. 85th edn, (CRC Press, 2004).
72 Sanfelix, P. C., Holloway, S., Kolasinski, K. W. & Darling, G. R. The structure of water on the (0001) surface of graphite. *Surf. Sci.* **532**, 166-172, doi: 10.1016/S0039-6028(03)00161-4 (2003).
73 Bolina, A. S., Wolff, A. J. & Brown, W. A. Reflection absorption infrared spectroscopy and temperature-programmed desorption studies of the adsorption and desorption of amorphous and crystalline water on a graphite surface. *J. Phys. Chem. B* **109**, 16836-16845, doi:10.1021/jp0528111 (2005).

74 Chakarov, D. V., Osterlund, L. & Kasemo, B. Water-Adsorption on Graphite(0001). *Vacuum* **46**, 1109-1112 (1995).
75 Löfgren, P., Ahlström, P., Lausma, J., Kasemo, B. & Chakarov, D. Crystallization Kinetics of Thin Amorphous Water Films on Surfaces. *Langmuir* **19**, 265-274, doi:10.1021/la020218u (2002).
76 Lejonthun, L., Svensson, E. A., Andersson, P. U. & Pettersson, J. B. C. Formation of Adsorbed Layers by Deposition of Dinitrogen Pentoxide, Nitric Acid, and Water on Graphite. *J. Phys.Chem. C* **113**, 7728-7734, doi:10.1021/jp809866z (2009).
77 Suter, M. T., Andersson, P. U. & Pettersson, J. B. C. Formation of water-ammonia ice on graphite studied by elastic helium scattering. *Chem. Phys. Lett.* **445**, 208-212, doi:10.1016/j.cplett.2007.07.012 (2007).
78 Wolff, A. J., Carlstedt, C. & Brown, W. A. Studies of binary layered CH_3OH/H_2O ices adsorbed on a graphite surface. *J. Phys. Chem. C* **111**, 5990-5999, doi:10.1021/jp067377x (2007).
79 Morishige, K., Kawamura, K. & Kose, A. X-RAY-DIFFRACTION STUDY OF THE STRUCTURE OF A MONOLAYER METHANOL FILM ADSORBED ON GRAPHITE. *J. Chem.Phys.* **93**, 5267-5270 (1990).
80 Thomson, E. S., Kong, X. R., Andersson, P. U., Markovic, N. & Pettersson, J. B. C. Collision Dynamics and Solvation of Water Molecules in a Liquid Methanol Film. *J. Phys. Chem. Lett.* **2**, 2174-2178, doi: 10.1021/Jz200929y (2011).
81 Ulbricht, H., Zacharia, R., Cindir, N. & Hertel, T. Thermal desorption of gases and solvents from graphite and carbon nanotube surfaces. *Carbon* **44**, 2931-2942, doi: 10.1016/j.carbon.2006.05.040 (2006).
82 Lundgren, M., Allan, N. L. & Cosgrove, T. Wetting of water and water/ethanol droplets on a non-polar surface: A molecular dynamics study. *Langmuir* **18**, 10462-10466, doi: 10.1021/La026191w (2002).
83 Murphy, D. M. & Koop, T. Review of the vapour pressures of ice and supercooled water for atmospheric applications. *Q. J. Roy. Meteor. Soc.* **131**, 1539-1565, doi: 10.1256/Qj.04.94 (2005).
84 Koop, T., Luo, B. P., Tsias, A. & Peter, T. Water activity as the determinant for homogeneous ice nucleation in aqueous solutions. *Nature* **406**, 611-614, doi: 10.1038/35020537 (2000).
85 Trainer, M. G., Toon, O. B. & Tolbert, M. A. Measurements of Depositional Ice Nucleation on Insoluble Substrates at Low Temperatures: Implications for Earth and Mars. *J.Phys. Chem. C* **113**, 2036-2040, doi: 10.1021/Jp805140p (2009).
86 Shilling, J. E., Fortin, T. J. & Tolbert, M. A. Depositional ice nucleation on crystalline organic and inorganic solids. *J. Geophys. Res. Atmos.* **111**, doi: 10.1029/2005jd006664 (2006).
87 Vieceli, J., Roeselova, M. & Tobias, D. J. Accommodation coefficients for water vapor at the air/water interface. *Chem. Phys. Lett.* **393**, 249-255, doi: 10.1016/j.cplett.2004.06.038 (2004).
88 Kolb, C. E. *et al.* An overview of current issues in the uptake of atmospheric trace gases by aerosols and clouds. *Atmos. Chem. Phys.* **10**, 10561-10605, doi: 10.5194/acp-10-10561-2010 (2010).
89 Winkler, P. M. *et al.* Mass and thermal accommodation during gas-liquid condensation of water. *Phys. Rev. Lett.* **93**, doi: 10.1103/Physrevlett.93.075701 (2004).
90 Feistel, R. & Wagner, W. Sublimation pressure and sublimation enthalpy of H_2O ice Ih between 0 and 273.16 K. *Geochim. Cosmochim. Ac.* **71**, 36-45, doi: 10.1016/j.gca.2006.08.034 (2007).
91 Pratte, P., van den Bergh, H. & Rossi, M. J. The kinetics of H2O vapor condensation and evaporation on different types of ice in the range 130-210 K. *J. Phys. Chem. A* **110**, 3042-3058, doi: 10.1021/Jp053974s (2006).
92 Delval, C. & Rossi, M. J. The kinetics of condensation and evaporation of H2O from pure ice in the range 173-223 K: a quartz crystal microbalance study. *Phys. Chem. Chem. Phys.* **6**, 4665-4676, doi: 10.1039/B409995h (2004).
93 Fluckiger, B. & Rossi, M. J. Common precursor mechanism for the heterogeneous reaction of D_2O, HCl, HBr, and HOBr with water ice in the range 170-230 K: Mass accommodation coefficients on ice. *J. Phys. Chem. A* **107**, 4103-4115, doi: 10.1021/Jp021956u (2003).

94 Davy, J. G. & Somorjai, G. A. Studies of Vaporization Mechanism of Ice Single Crystals. *J. Chem. Phys.* **55**, 3624, doi: 10.1063/1.1676638 (1971).
95 Bartels-Rausch, T. *et al.* Ice structures, patterns, and processes: A view across the icefields. *Rev. Mod. Phys.* **84**, 885-944, doi: 10.1103/RevModPhys.84.885 (2012).
96 Tolbert, M. A. & Middlebrook, A. M. Fourier-Transform Infrared Studies of Model Polar Stratospheric Cloud Surfaces - Growth and Evaporation of Ice and Nitric-Acid Ice. *J. Geophys. Res. Atmos.* **95**, 22423-22431, doi: 10.1029/Jd095id13p22423 (1990).
97 Davis, A. & Strickland-Constable, R. F. in *Int. Symp. on Condensation and Evaporation of Solids.* 605-679.
98 Haynes, D. R., Tro, N. J. & George, S. M. Condensation and Evaporation of H2o on Ice Surfaces. *J. Phys. Chem.* **96**, 8502-8509 (1992).
99 Leu, M. T. Laboratory Studies of Sticking Coefficients and Heterogeneous Reactions Important in the Antarctic Stratosphere. *Geophys. Res. Lett.* **15**, 17-20 (1988).
100 Kramers, H. & Stemerding, S. The Sublimation of Ice in Vacuum. *Appl. Sci. Res.* **3**, 73-82 (1951).
101 Delval, C., Fluckiger, B. & Rossi, M. J. The rate of water vapor evaporation from ice substrates in the presence of HCl and HBr: implications for the lifetime of atmospheric ice particles. *Atmos. Chem. Phys.* **3**, 1131-1145 (2003).
102 Chaix, L., van den Bergh, H. & Rossi, M. J. Real-time kinetic measurements of the condensation and evaporation of D2O molecules on ice at 140K < T < 220K. *J. Phys. Chem. A* **102**, 10300-10309, doi: 10.1021/Jp983050n (1998).
103 Isono, K. & Iwai, K. Growth Mode of Ice Crystals in Air at Low Pressure. *Nature* **223**, 1149-1150 (1969).
104 Earle, M. E., Kuhn, T., Khalizov, A. F. & Sloan, J. J. Volume nucleation rates for homogeneous freezing in supercooled water microdroplets: results from a combined experimental and modelling approach. *Atmos. Chem. Phys.* **10**, 7945-7961, doi: 10.5194/acp-10-7945-2010 (2010).
105 Magee, N., Moyle, A. M. & Lamb, D. Experimental determination of the deposition coefficient of small cirrus-like ice crystals near-50 degrees C. *Geophys. Res. Lett.* **33**, doi:10.1029/2006gl026665 (2006).
106 Choularton, T. W. & Latham, J. Measurements of Deposition Coefficient for Ice, and Its Application to Cirrus Seeding. *Q. J. Roy. Meteor. Soc.* **103**, 307-318, doi: 10.1002/qj.49710343608 (1977).
107 Wren, S. N. & Donaldson, D. J. Exclusion of Nitrate to the Air-Ice Interface During Freezing. *J. Phys. Chem. Lett.* **2**, 1967-1971, doi: 10.1021/Jz2007484 (2011).
108 Barnes, G. T. Permeation through monolayers. *Coll. Surf. A* **126**, 149-158, doi:10.1016/s0927-7757(96)03926-x (1997).
109 Lamer, V. K., Aylmore, L. A. G. & Healy, T. W. Transport of Water through Monolayers of Long-Chain N-Paraffinic Alcohols. *J. Coll. Sci.* **19**, 673, doi: 10.1016/0095-8522(64)90075-3 (1964).
110 Gilde, A., Siladke, N. & Lawrence, C. P. Molecular Dynamics Simulations of Water Transport through Butanol Films. *J. Phys. Chem. A* **113**, 8586-8590, doi: 10.1021/Jp9026699 (2009).
111 Lawrence, J. R., Glass, S. V. & Nathanson, G. M. Evaporation of water through butanol films at the surface of supercooled sulfuric acid. *J. Phys. Chem. A* **109**, 7449-7457, doi: 10.1021/Jp050042f (2005).
112 Brunauer, S., Deming, L. S., Deming, W. E. & Teller, E. On a theory of the van der Waals adsorption of gases. *J. Am. Chem. Soc.* **62**, 1723-1732, doi: 10.1021/Ja01864a025 (1940).
113 Miles, R. E. H., Reid, J. P. & Riipinen, I. Comparison of Approaches for Measuring the Mass Accommodation Coefficient for the Condensation of Water and Sensitivities to Uncertainties in Thermophysical Properties. *J. Phys. Chem. A*, doi:10.1021/jp3083858 (2012).